



Shear and torsion interaction of hollow core slabs

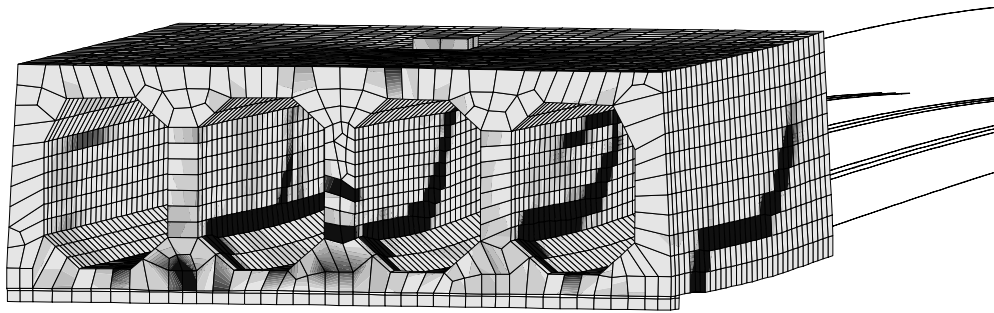
HOLCOTORS

Technical Report 1

Finite element analyses of hollow core units subjected to shear and torsion

December 2002

CHALMERS



Finite Element Analyses of Hollow Core Units Subjected to Shear and Torsion

HELÉN BROO, KARIN LUNDGREN

Department of Structural Engineering

Concrete Structures

CHALMERS UNIVERSITY OF TECHNOLOGY

Göteborg, Sweden 2002

Report No. 02:17

REPORT NO. 02:17

Finite Element Analyses of Hollow Core Units Subjected to Shear and Torsion

HELÉN BROO, KARIN LUNDGREN

Department of Structural Engineering
Concrete Structures
CHALMERS UNIVERSITY OF TECHNOLOGY
Göteborg, Sweden 2002

Finite Element Analyses of Hollow Core Units Subjected to Shear and Torsion

HELÉN BROO, KARIN LUNDGREN

© HELÉN BROO, KARIN LUNDGREN, 2002

ISSN 1650-5166

Report no. 02:17

Archive no. 82

Department of Structural Engineering

Concrete Structures

Chalmers University of Technology

SE-412 96 Göteborg

Sweden

Telephone: + 46 (0)31-772 1000

Cover:

Crack pattern from the analysis of the test ST400C.

Department of Structural Engineering

Göteborg, Sweden 2002

Finite Element Analyses of Hollow Core Units Subjected to Shear and Torsion

HELÉN BROO, KARIN LUNDGREN

Department of Structural Engineering

Concrete Structures

Chalmers University of Technology

ABSTRACT

Precast prestressed hollow core units are among the most advanced and widely spread products in the precast industry. The present calculation method for shear and torsion in hollow core slabs adds stresses from various influences without considering deformations and compatibility, the softening of cracking concrete, or restraint at the boundaries, and is therefore most likely conservative. The aim of this work is to improve the current knowledge and understanding of shear and torsion interaction in hollow core floors.

This report deals with finite element analyses of individual hollow core units, subjected to different combinations of shear and torsion. Most of these analyses concern full-scale tests on hollow core units that were planned in cooperation with VTT and Strängbetong, and conducted at VTT during June and August 2002. Prestressed hollow core units of two thicknesses, 200 mm and 400 mm, were tested both with and without eccentric loading. The analyses were made with various levels of detailing, using the finite element program DIANA 7.2.

The aim was to use a modelling technique that does not result in too time consuming analyses, but still gives a reasonable good agreement. In the final analyses presented here, only the part of the slab closest to the load and the active support was modelled with solid elements. The rest of the slab was modelled with beam elements. The concrete was modelled using non-linear fracture mechanics in a smeared rotating crack model.

In general the finite element analyses of the tests were able to capture the overall behaviour, failure mode, crack pattern, and maximum obtained load, with a reasonably good agreement, though a very coarse mesh were used in the analyses. Especially for the centrally loaded specimens, the agreement was good. However, for the eccentrically loaded hollow core units the maximum load was overestimated. The reason for this is most likely that the torsional stiffness of the beam elements used in the model was too high.

Key words: prestressed concrete, hollow core slab, hollow core unit, finite element analyses, non-linear analyses, shear, torsion.

Contents

ABSTRACT	I
CONTENTS	I
PREFACE	III
1 INTRODUCTION	1
2 EXPERIMENTAL TESTS	2
2.1 Test programme	2
2.2 Shear tension tests	4
2.3 Shear flexure test	7
2.4 Pure torsion tests	8
3 FINITE ELEMENT ANALYSES	10
3.1 Development of the finite element model	10
3.2 Modelling of materials	17
4 COMPARISON OF TESTS AND ANALYSES	21
4.1 Analyses of shear tension tests on the 200 mm thick units.	21
4.1.1 Analysis of the test ST200C	23
4.1.2 Analysis of the tests ST200E1 and ST200E1b	25
4.1.3 Analysis of the test ST200E2	26
4.2 Analyses of shear tension tests on the 400 mm thick units	28
4.2.1 Analysis of the test ST400C	30
4.2.2 Analysis of the test ST400C2	33
4.2.3 Analysis of the test ST400E1	36
4.3 Discussion of the analyses of shear tension tests	40
4.4 Analyses aiming at shear flexure failure	41
5 CONCLUSIONS	47
6 REFERENCES	48
APPENDIX A	1

Preface

In this study, finite element analyses of prefabricated prestressed single hollow core units subjected to shear and torsion were carried out. The analyses were carried out from January 2002 to December 2002. The work is part of a research project concerning interaction of shear and torsion in hollow core floors. The project is financed by the 5th Framework of European Commission; the International Prestressed Hollow Core Association; the Bundesverband Spannbeton-Hohlplatten, Germany, and VTT.

This part of the project was carried out at the Department of Structural Engineering, Concrete Structures, Chalmers University of Technology, Sweden, with Civ. Ing. Helén Broo as a researcher; Ass. Prof. Karin Lundgren as a researcher and assistant supervisor and Prof. Björn Engström as supervisor.

The photographs in this report are used with kind permission of VTT. We would like to thank Matti Pajari at VTT for letting us use the data collected during the tests directly after the tests were carried out.

Göteborg December 2002

Helén Broo

Karin Lundgren

1 Introduction

Precast prestressed hollow core slabs are among the most advanced and widely spread products in the precast industry. Concentrated loads on a single hollow core unit are transversely distributed to the surrounding units by the shear keys in the longitudinal joints. Normally, the joints between hollow core units crack and are assumed to act as hinges. Consequently, load distribution to the neighbouring units always introduces a torsional moment. Torsional loading on a hollow core unit produces shear stresses in the perimetric zone of the unit. These shear stresses act upwards in one and downwards in the other of the outermost webs. The stresses are to be cumulated with those resulting from the ordinary vertical shear force, which is uniformly distributed over the webs. This means that one web in the cross-section receives much more stresses than the other ones; however there is most likely a certain redistribution of stresses between the webs. Studies and tests carried out by Gabrielsson (1999) indicated that such redistribution exists. The present calculation method for shear and torsion in hollow core units adds stresses from various influences without considering deformations and compatibility within the unit, the softening of cracking concrete, or restraint at the boundaries of the considered element.

The aim of this project is to improve the current knowledge and understanding of, and to develop a design method for, shear and torsion interaction in hollow core floors. To reach this goal, experiments are combined with finite element analyses, using non-linear fracture mechanics. Both individual hollow core units and floors are investigated.

The project is carried out in different steps, starting from the modelling and testing of hollow core units and complete floors, followed by parameter studies, and the elaboration of a design method. Experimental studies and development of finite element models are carried out simultaneously and in an interactive way so that the information needed in the models is searched for in the experiments by successive improvements of the measuring and testing techniques. Chalmers University of Technology, Department of Structural Engineering, is carrying out the modelling. The experimental work is carried out by VTT, the Technical Research Centre of Finland.

This report presents results from the first part of the project that deals with finite element analyses of hollow core units. The results from the analyses are compared with those from the corresponding tests. The experimental tests were performed at VTT in June and August 2002. The tests are reported by Pajari (2003a) and Pajari (2003b). The tests are here briefly presented in Chapter 2. In Chapter 3, the development of the finite element models is described, and the results from the final analyses are compared with those from the experiments in Chapter 4.

2 Experimental Tests

2.1 Test programme

Most of the analyses presented in this report are of full-scale experimental tests on hollow core units that were planned in cooperation with VTT and Strängbetong, and conducted at VTT during June and August 2002. The tests are reported by Pajari (2003a) and Pajari (2003b). The tests are here briefly presented and some of the results are compared with those from the analyses in Chapter 4.

Hollow core units are produced in thicknesses from 100 mm to 500 mm, with different sectional geometries and various amounts of reinforcement or prestressing steel FIP (1998). The hollow core units are either extruded or slip-formed. Within this project 200 mm and 400 mm thick extruded hollow core units and 200 mm thick slip formed hollow core units were tested both with and without eccentric loading. All tested hollow core units were prestressed. The different geometries for the extruded units can be seen in Figure 2.1 and Figure 2.2.

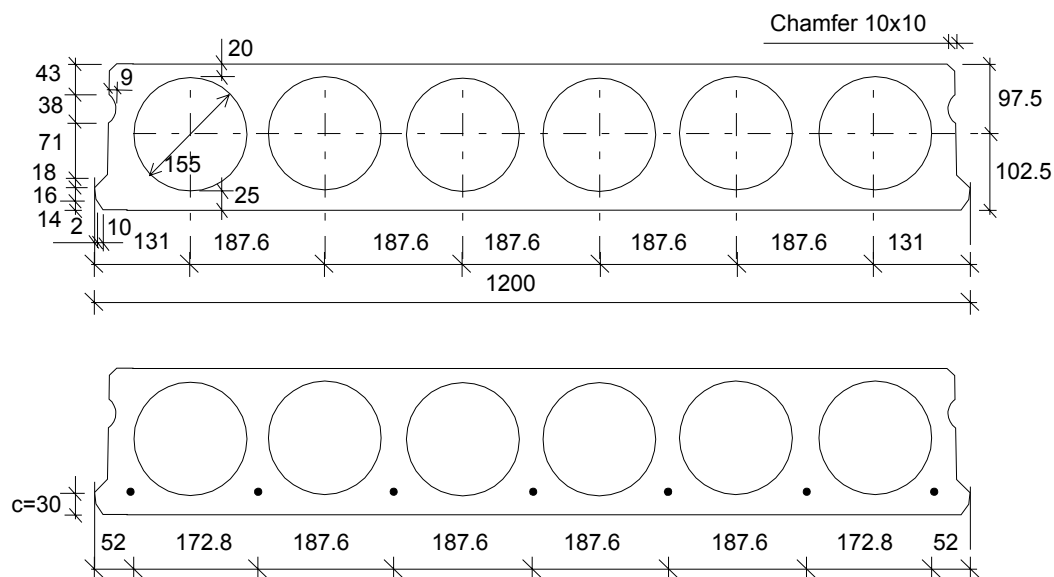


Figure 2.1 Cross-section of the 200 mm thick extruded hollow core unit, adopted from Pajari (2003a).

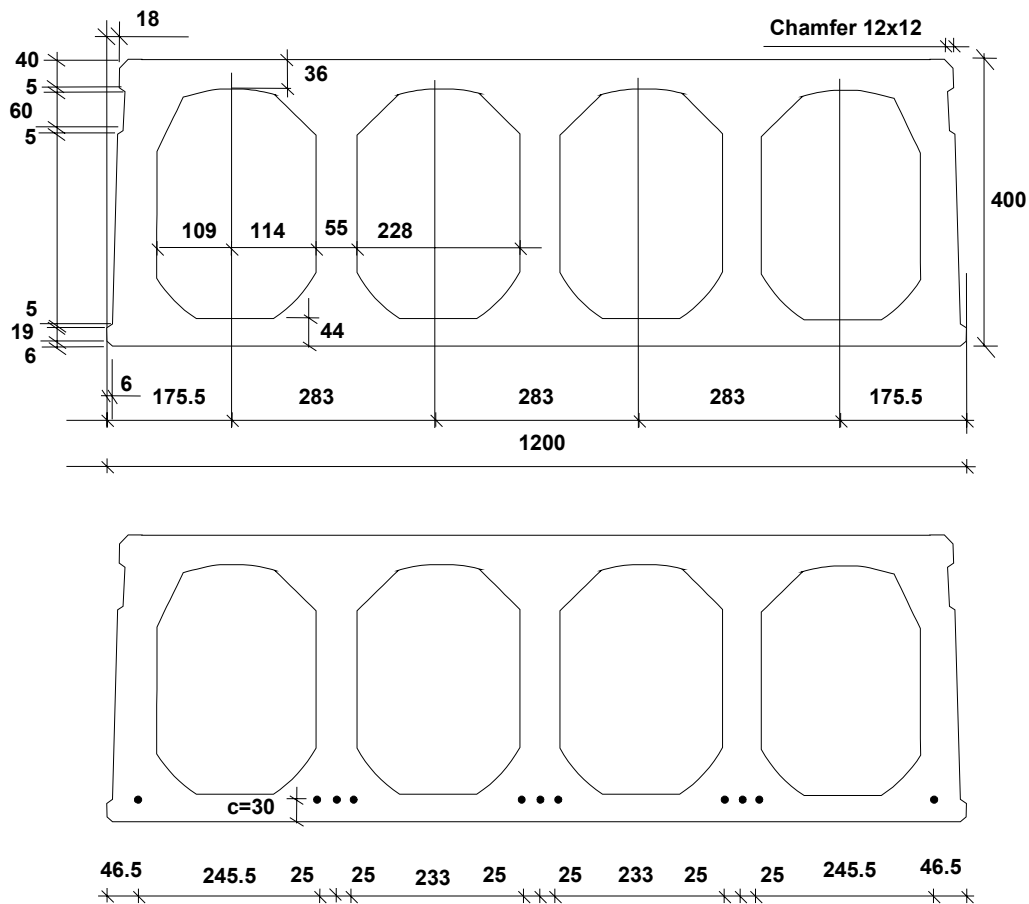


Figure 2.2 Cross-section of the 400 mm thick extruded hollow core unit, adopted from Pajari (2003b).

To evaluate the effects of torsion in combination with a shear force the hollow core units were loaded with one or two point loads placed with different eccentricities. In order to avoid local failures such as punching through, the loads were never placed over two neighbouring webs. According to the prEN 1168 CEN/TC229 (2000) and the literature, e.g. Pajari (1989), two different shear failure modes could appear in hollow core units, shear tension failure and shear flexure failure, sometimes also named as shear compression failure. The latter is more likely to appear in thick slabs and was therefore only tested on the 400 mm thick hollow core unit. The test program is shown in Table 2.1.

Table 2.1 Test programme.

	Thickness h [mm]	Type	Length [m]	Span l [m]	Number of tests
Torsion tests	200	Extruded	5	4	2
	400	Extruded	7	6	2
Shear tension tests	200	Extruded	7.06	7	4
	200	Slip formed	7.06	7	2
	400	Extruded	7.08	7	4
Shear flexure tests	400	Extruded	7.08	7	1
Total number of tests					15

2.2 Shear tension tests

These tests were made to provoke a shear tension failure in the webs of the hollow core units. The principal testing arrangement for the shear tension tests is shown in Figure 2.3 and Figure 2.4. The shear span was chosen to $x = 2.5h$ according to the test method specified in prEN 1168 Annex K, see CEN/TC229 (2000). Since the length of the span does not affect the shear failure, equal lengths of span were chosen for all tests. The support lengths for the 200 mm thick hollow core units were 60 mm and for the 400 mm thick units 80 mm. A 10 mm thick soft bearing strip of neoprene was placed between the support and the hollow core unit. The vertical displacement of the hollow core unit was measured in two points over each support and over each web at a distance b from the load. For the 200 mm thick hollow core units $b = 100$ mm and for the 400 mm thick $b = 200$ mm. The tests are described more in detail in Pajari (2003b). Details about the shear tension tests and the test specimens are shown in Table 2.2 for the 200 mm thick units and in Table 2.3 for the 400 mm thick units.

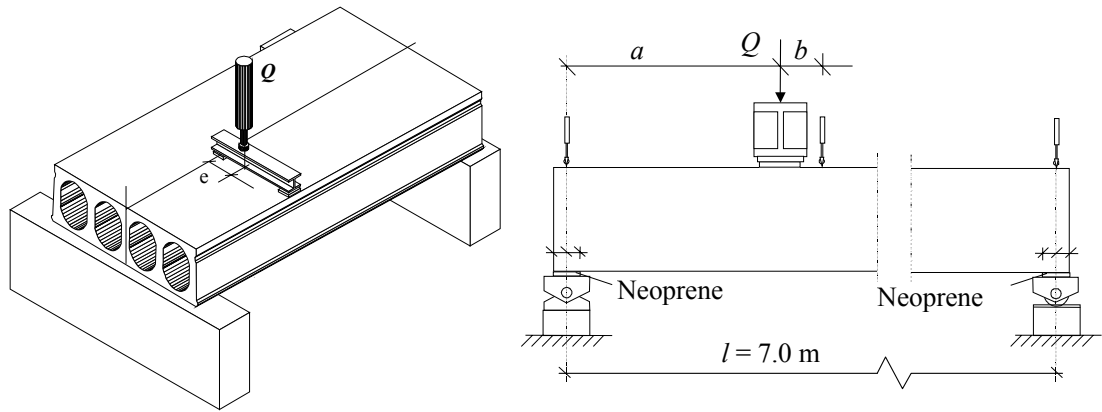


Figure 2.3 *Principal testing arrangement for the shear tension tests, modified from Pajari (2003b).*

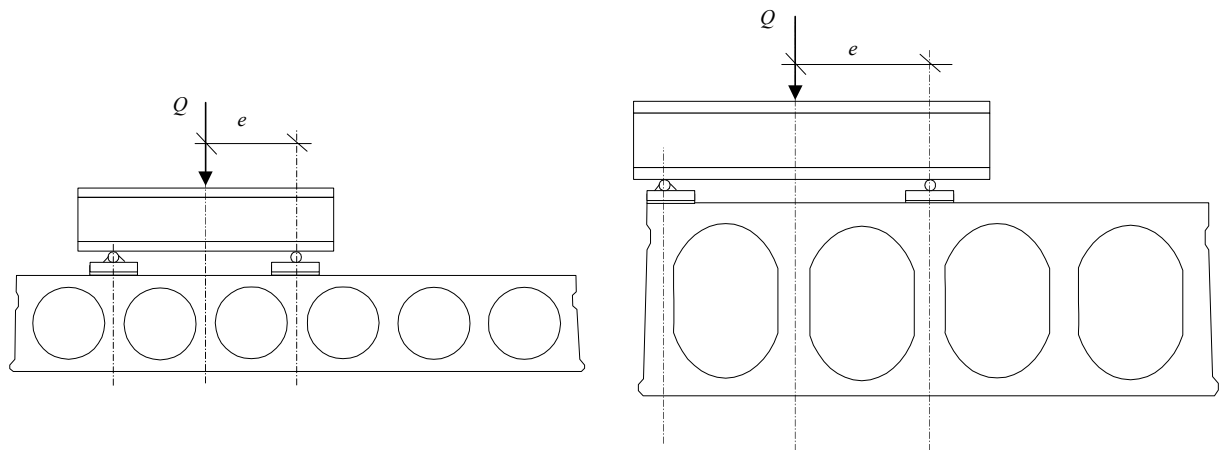
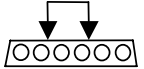
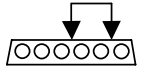
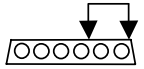
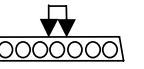
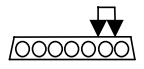


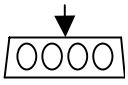
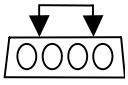
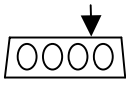
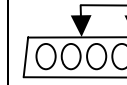
Figure 2.4 *Arrangement of the load distribution beam in relation to the web locations for the 200 mm thick unit and for the 400 mm thick unit, modified from Pajari (2003b).*

Table 2.2 Shear tension tests on the 200 mm thick hollow core units.

Test identification	ST200C	ST200E1	ST200E2	STS200C	STS200E1
					
Type	Extruded	Extruded	Extruded	Slip formed	Slip formed
Thickness h [mm]	200	200	200	200	200
Number of strands	7	7	7	8 and 6*	8 and 6*
Diameter of strand \varnothing [mm]	12.5	12.5	12.5	12.5 and 5*	12.5 and 5*
Initial prestress [MPa]	900	900	900	900 and 700*	900 and 700*
Length of slab [m]	7.06	7.06	7.06	7.06	7.06
Length of span l [m]	7	7	7	7	7
Length of shear span a [m]	0.5	0.5	0.5	0.5	0.5
Eccentricity e [m]	0	0.187	0.374	0	0.314
Number of tests	1	2	1	1	1

*Prestressing wires in the top flange of the slip-formed hollow core unit.

Table 2.3 Shear tension tests on the 400 mm thick hollow core units.

Test identification	ST400C1	ST400C2	ST400E1	ST4002E
				
Type	Extruded	Extruded	Extruded	Extruded
Thickness h [mm]	400	400	400	400
Number of strands	11	11	11	11
Diameter of strand \varnothing [mm]	12.5	12.5	12.5	12.5
Initial prestress [MPa]	1000	1000	1000	1000
Length of slab [m]	7.08	7.08	7.08	7.08
Length of span l [m]	7	7	7	7
Length of shear span a [m]	1.0	1.0	1.0	1.0
Eccentricity e [m]	0	0	0.283	0.283
Number of tests	1	1	1	1

2.3 Shear flexure test

One test was made to provoke a shear flexure failure. This failure mode starts with a bending crack that turns into an inclined crack, and ends with a shear displacement along the crack. The testing arrangement for this test is shown in Figure 2.5. Details about the test and the test specimen are shown in Table 2.4. The test is described more in detail in Pajari (2003b).

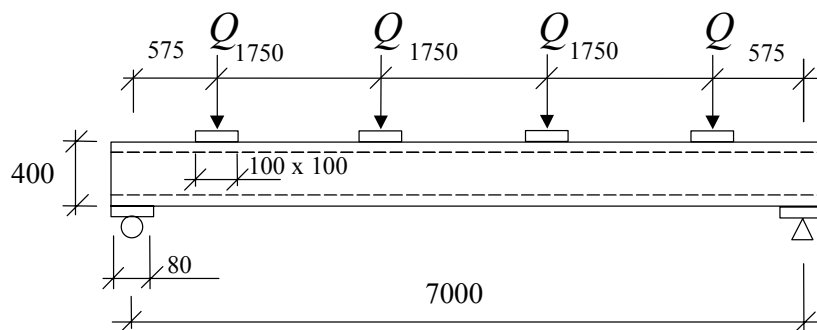
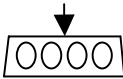


Figure 2.5 Principal test arrangement for the shear flexure test.

Unfortunately this test did not turn out in the way it was planned. Instead the result was an abrupt shear tension failure. Even so, some analyses were made to investigate the possibility to obtain a shear flexure failure, see Chapter 4.4.

Table 2.4 Shear flexure test on the 400 mm thick hollow core unit.

Test identification	SF400C
	
Type	Extruded
Thickness h [mm]	400
Number of strands	11
Diameter of strand \varnothing [mm]	12.5
Initial prestress [MPa]	1000
Length of slab [m]	7.08
Length of span l [m]	7
Length of shear span $a=l/4$ [m]	1.75
Eccentricity e [m]	0
Number of tests	1

2.4 Pure torsion tests

The pure torsion tests were carried out to evaluate the torsional resistance of the hollow core units. The principal testing arrangement is shown in Figure 2.6. Details about the tests and the test specimens are shown in Table 2.5. The tests are described more in detail in Pajari (2003a).

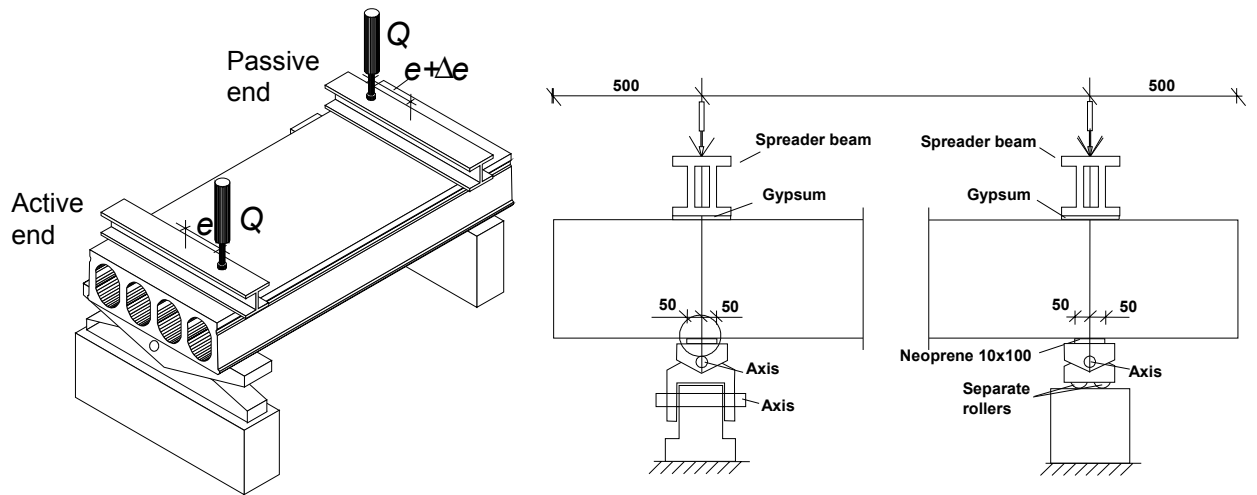


Figure 2.6 Principal testing arrangement for the pure torsion tests, modified from Pajari (2003a).

Table 2.5 Pure torsion test on the hollow core units.

Test identification	PT200A, PT200B	PT400A, PT400B
		
Type	Extruded	Extruded
Thickness h [mm]	200	400
Number of strands	7	7
Diameter of strand \varnothing [mm]	12.5	12.5
Initial prestress [MPa]	900	1000
Length of slab [m]	5.0	7.0
Length of span l [m]	4.0	6.0
Length of cantilever [m]	0.5	0.5

3 Finite Element Analyses

The finite element analyses described here were performed at Chalmers University of Technology during January to December 2002. Hollow core units subjected to different combinations of shear and torsion were modelled with various levels of detailing, using the non-linear finite element program DIANA 7.2. The work started with modelling of tests of hollow core units subjected to shear and torsion available in the literature. The information and knowledge gained from these analyses was then used when preliminary analyses for planning purposes were done, in order to decide a test plan. After these tests had been conducted at VTT, during June and August 2002, more detailed analyses were carried out. Due to discovered disadvantages with these models, they were further developed. In this chapter, first the development of these models is described. Thereafter, the material models used are described. The results from the final analyses are compared with test results in Chapter 4.

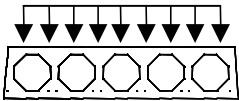
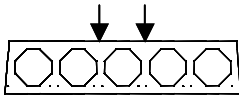
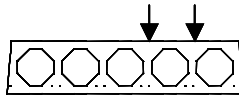
3.1 Development of the finite element model

As described above, several versions of finite element models have been established and tested.

1. At first analyses of tests carried out at Luleå Technical University by Gabrielsson (1999) were made. An overview of the tests is shown in Table 3.1. The aim with these analyses was to get a first idea of how detailed the analyses need to be, and how coarse mesh that can be used, in order to describe the reality in a sufficient good way. The tested hollow core slab units were modelled with a coarse mesh of solid elements and full interaction between the prestressing strands and the concrete, see Figure 3.1. The nodes at the edges were supported for vertical deformation, as shown in Figure 3.1, and each point load was applied on two nodes with load control. For these models all necessary material data were taken from Gabrielsson (1999). A typical load versus displacement relation from these analyses is shown in Figure 3.2. In all of these analyses, convergence was obtained until cracking of the webs occurred. Thereafter, the load could still be increased; however, the equilibrium iteration did not converge in the analyses. Therefore, it was judged that the following increase of the load was not reliable and, consequently, the maximum load from the analysis was evaluated as the one when the webs cracked. In Figure 3.3, these evaluated maximum loads are compared to the ones measured in the tests. As can be seen, there is a rather good agreement. The conclusions from these analyses concerning future analyses were:

- This type of modelling appears to give a reasonable description of the overall behaviour when comparing crack pattern, deflections, and maximum load.
- If the response after maximum load is of interest, the interaction between the prestressing steel and the concrete must be included, for example by using a bond-slip relation.

Table 3.1 Overview of analyses of tests carried out by Gabrielsson (1999).

			
Normal strength concrete	B1	B2	B4
High strength concrete	B3H	B2H	B4H

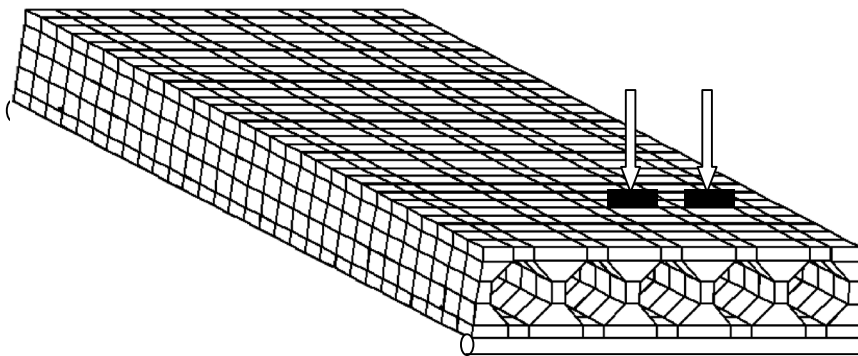


Figure 3.1 Mesh used for the analyses of tests carried out by Gabrielsson (1999). Loading shown is as in analysis of specimen B4 and B4H.

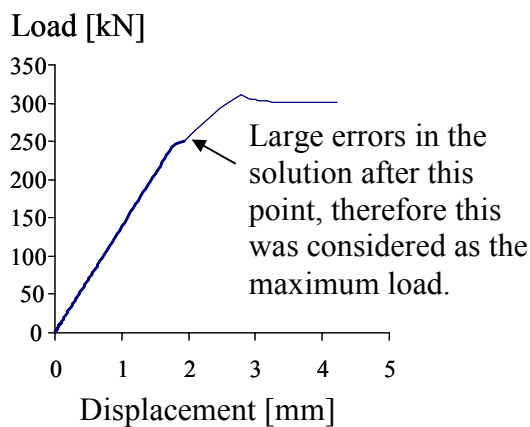


Figure 3.2 Load versus displacement at the centre of the cross-section where the load was applied from the analysis of test specimen No. B2 reported in Gabrielsson (1999).

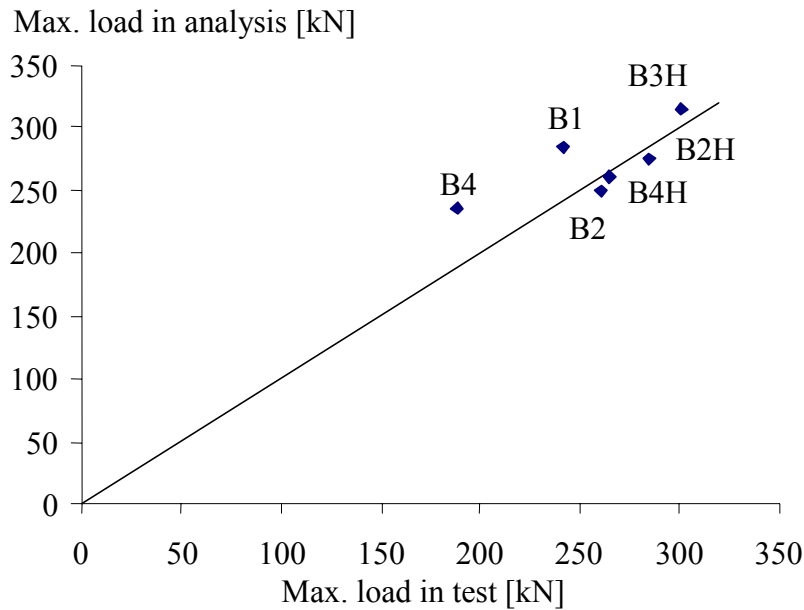


Figure 3.3 Evaluated maximum loads in analyses compared to the measured ones in the tests by Gabrielsson (1999).

2. Before planning the test program and deciding the test specimens and the testing arrangements, analyses aiming at shear tension failure and pure torsion failure were made on 200 mm thick hollow core units. The main aim with these analyses was to get background information to decide the test plan. The hollow core unit was modelled with a coarse mesh and full interaction between prestressing steel and concrete. The whole unit was modelled with eight node solid elements, see Figure 3.4. In the analyses aiming at shear tension failure, the loads were applied directly on single concrete nodes with load control, and the bottom nodes of the edge sections were supported for vertical deformation. In Figure 3.5, the load versus displacement curves obtained in these analyses are shown. In the analyses aiming at pure torsion failure, the nodes on one of the edges were tied for vertical deformation. At the other edge of the hollow core unit, the upper and lower nodes were tied to remain at straight lines, and to rotate around a centre node. A vertical force was applied on the outermost edge node, resulting in a pure torsional moment. Some results from the analyses made for the pure torsion tests are compared with test results in Figure 3.6. The conclusions from these analyses concerning future analyses were:

- In the pure torsion tests, the placement of the supports of the hollow core unit was chosen to be 0.5 m from the free edges. Thereby, full interaction between the prestressing steel and the concrete can be assumed in the analyses.
- As concluded also from the analyses of the tests by Gabrielsson (1999), the interaction between the prestressing steel and the concrete must be included, for example by using a bond-slip relation, if the response after maximum load at a shear tension failure is of interest.

- Modelling the whole slab with solid elements resulted in a very large model and time-consuming analyses. Simplifications of the model are necessary.

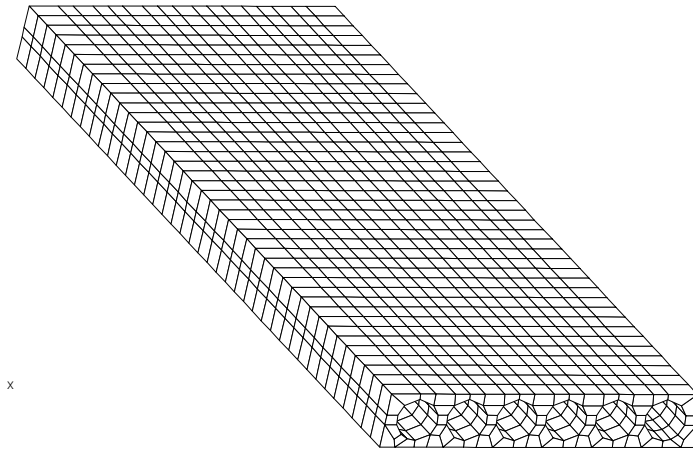


Figure 3.4 Mesh used for preliminary analyses.

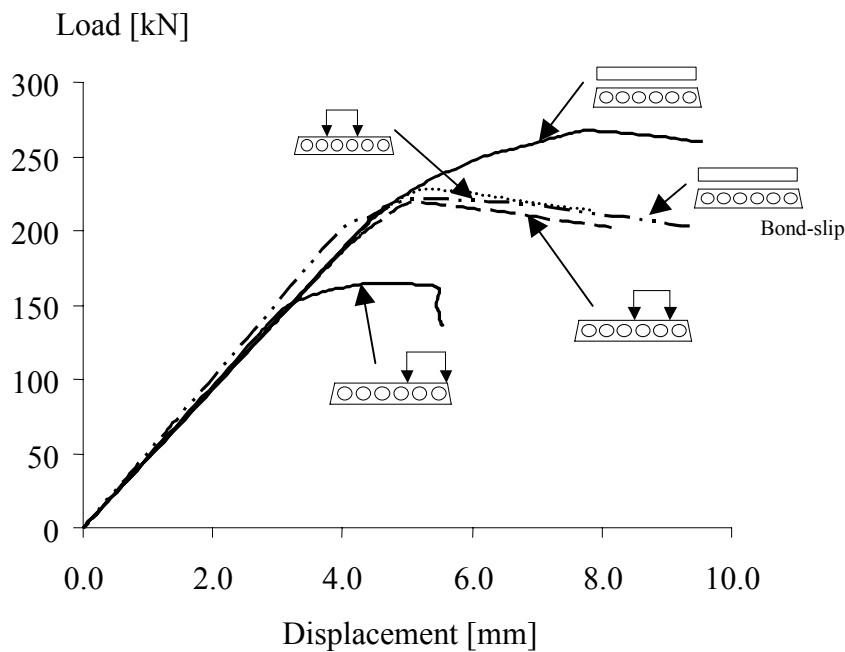


Figure 3.5 Load versus displacement at the centre of the cross-section where the load was applied, for different load cases from preliminary analysis for the 200 mm thick hollow core unit.

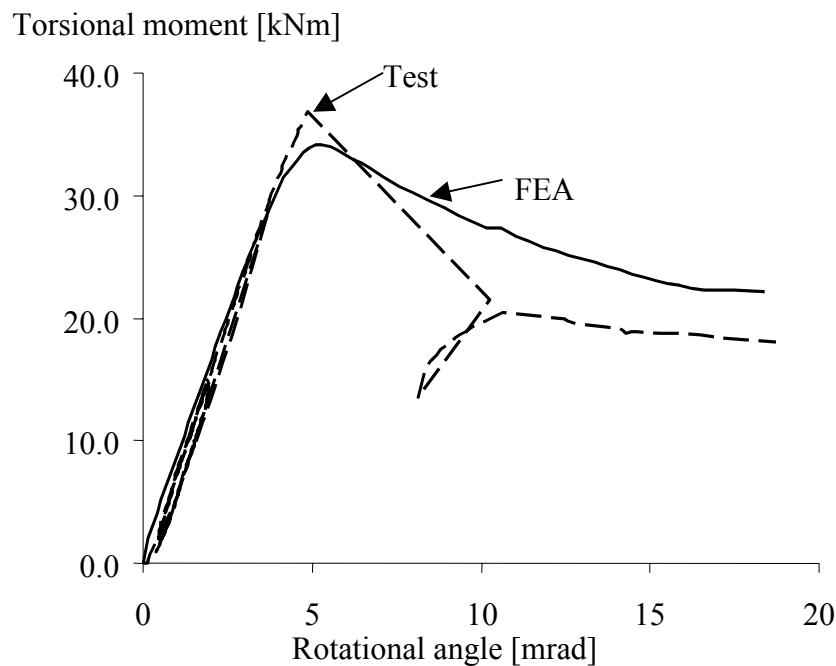


Figure 3.6 Comparison of test result and analysis of pure torsion test PT200A; Torsional moment versus rotational angle.

3. The aim with the following analyses was to improve the modelling technique, so that a reasonable good agreement could be obtained with less time consuming analyses. Therefore, these analyses were made on models where only the part of the hollow core unit closest to the load and the active support, 1.03 m and 1.54 m respectively, was modelled with eight-node solid elements. The rest of the slab was modelled with three-node beam elements, as shown in Figure 3.9. The solid elements were connected to the beam elements by assuming that the plane cross-section remained plane, and a stiff rotation of the cross-section. The cross-section in the beam elements was described with zones, as shown in Figure 3.7. In the part with solid elements, the strands were modelled with two-node bar elements, combined with interface elements and a bond-slip relation to simulate the interaction between the prestressing steel and the concrete. In the part of the model with beam elements, the strands were modelled as embedded reinforcement. This choice means that in the beam elements, full interaction between the prestressing steel and the concrete was assumed. When using a bond-slip relation between the strands and the concrete, special consideration must be taken when modelling the support. If support is applied only on the edge nodes, as was done in the earlier analyses, the reinforcement would not be anchored at the support. This would lead to numerical instabilities. Therefore, the support plate was modelled with eight-node solid elements. The same was done also for the loading plates, in order to spread the applied load over several nodes to avoid local failure. Between the loading plates and the concrete, as well as between the support plate and the concrete, full interaction was assumed. At the support plates, the nodes situated on the line in the centre of the support plate were supported for

vertical deformation, thus enabling a rotation and simulating a free support. The loads were applied, with load control, as point loads acting at the centre node of the loading plates. Both the 200 mm and the 400 mm thick slabs were modelled and analysed this way. A typical example of a load versus displacement relation from these analyses is shown in Figure 3.8. As can be seen, both the stiffness and the maximum load were largely overestimated. The conclusions from these analyses concerning future analyses were:

- When the loading is eccentric, lifting of the slab at the support must be allowed.
- The deformation of the supports was large in the tests, due to the neoprene strips used. Either the test results must be adjusted to account for this, or the neoprene must be included in the analyses.

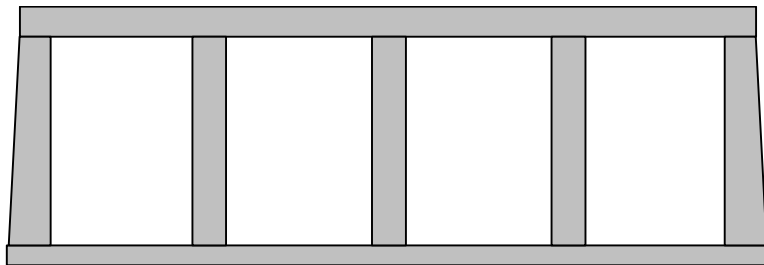


Figure 3.7 The cross-section in the beam elements in the analyses of hollow core units with a thickness of 400 mm, described with zones.

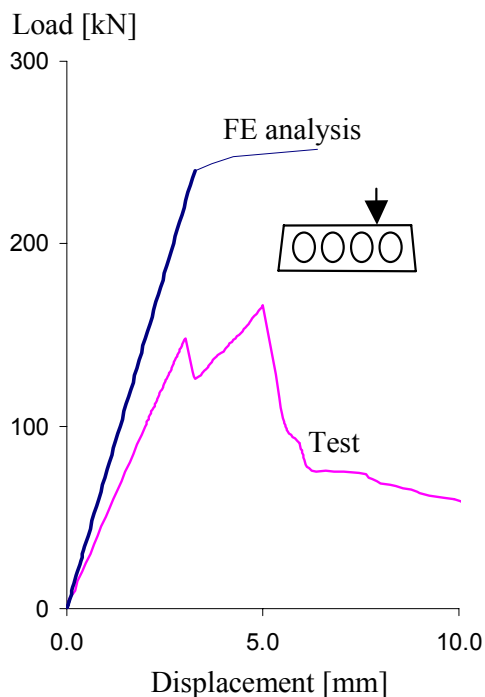


Figure 3.8 Load versus displacement at the centre of the cross-section close to the load in the same point as the displacement was measured in the test. Results from test and analysis of test specimen ST400E1.

again. An example of the mesh used is shown in Figure 3.10. These analyses are in this report denoted “the final analyses”. Results from these analyses are presented in Chapter 4.

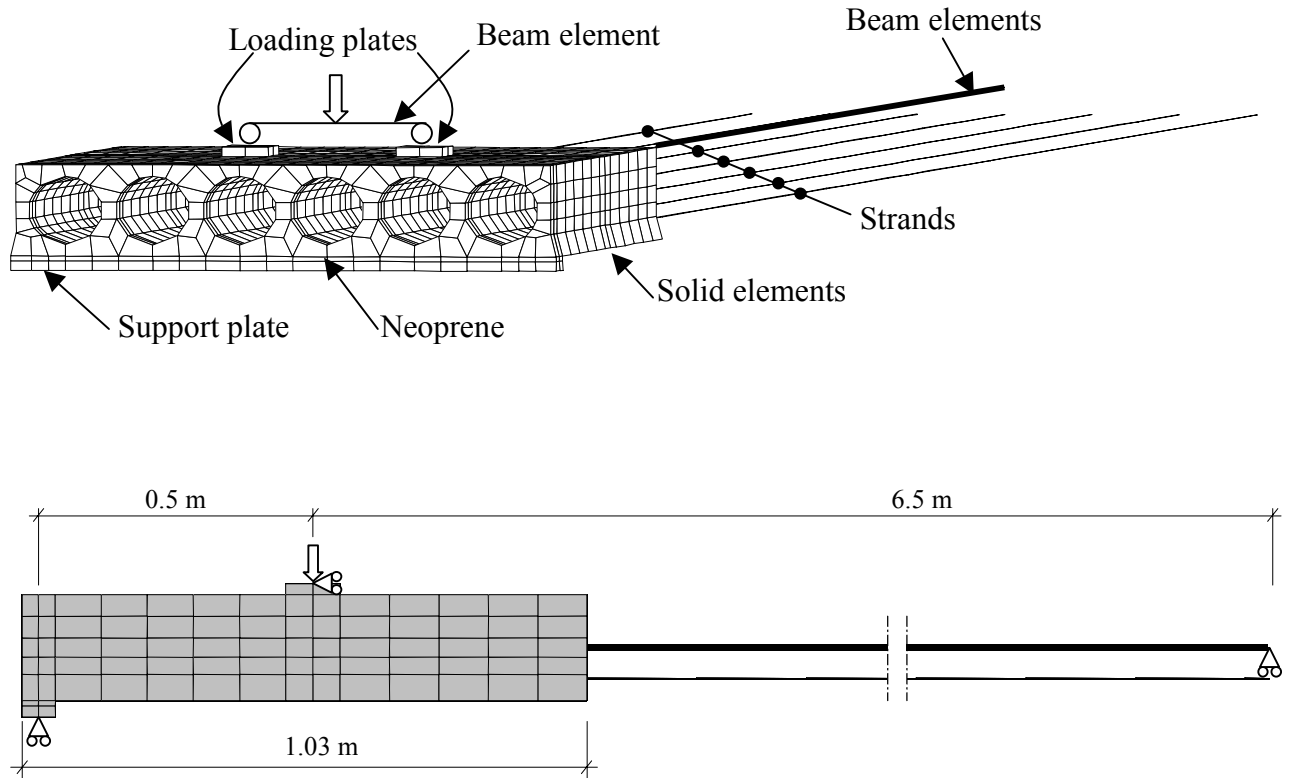


Figure 3.10 Mesh used in the final analysis of ST200C test carried out at VTT.

3.2 Modelling of materials

In all of the analyses, the concrete was modelled with a constitutive model based on non-linear fracture mechanics. A rotating crack model based on total strain was used for the concrete, see TNO (1998). The hardening in compression was described by the expression of Thorenfeldt and for the tension softening, the curve by Hordijk was chosen, as described in TNO (1998), see Figure 3.11. Material data for the concrete were calculated from the compressive cylinder tests on 50 mm cores drilled from the tested specimens, carried out by VTT, see Pajari (2003a) and Pajari (2003b). It was assumed that the measured mean compressive strength, $f_{ccm,C50}$, directly gives the corresponding strength for 150 mm cub, $f_{ccm,cube}$. Furthermore it was assumed that the 150 mm cylinder strength, $f_{ccm,C150}$, is equal to 85 % of the cube strength, according to Byggtjänst (1994). From this value, the mean tensile strength, f_{ctm} , was calculated according to CEB (1995); the fracture energy, G_F , and the Young’s modulus, E_{ci} , were calculated according to CEB (1993). The values used for the different models are shown in Table 3.2. The fracture energy is calculated for a maximum aggregate size of 16 mm. The maximum aggregate size in the concrete used for the 200 mm thick

hollow core units was 12 mm, this gives $G_F = 92.4 \text{ Nm/m}^2$ instead of $G_F = 100.7 \text{ Nm/m}^2$ that was used in these analyses.

The constitutive behaviour of the prestressing steel was modelled by the von Mises yield criterion with an associated flow law and isotropic hardening, using the strength and modulus of elasticity measured in tensile tests carried out at VTT, see Pajari (2003b). The stress strain relationship for the strand used in the models is shown in figure 3.12. The tensile strengths, $f_{0.1u}/f_{pu}$, and the Young's modulus, E_p , for the prestressing steel are shown in Table 3.2.

The bond-slip relationship between seven wire strands and concrete, see Figure 3.13, was taken from pull-through tests carried out at Chalmers, Lundgren (2002). In reality, the bond-slip relation depends on the surrounding structure. For example, the bond stress is decreased if splitting of the concrete occurs, and increased at release of the prestressing force and at the support region due to the increased normal stresses between the concrete and the steel. However, it was accepted as a reasonable simplification to use the same bond-slip relation for all load cases.

To evaluate the stiffness of the 10 mm thick neoprene, two loading tests, one with and one without neoprene, were performed at VTT. The loaded area in these tests was $80 \times 500 \text{ mm}^2$. The difference in stiffness between these two tests was then evaluated and used as input for the stiffness of the neoprene in the analyses, $K = 6.7 \text{ GPa/m}$, see Figure 3.14.

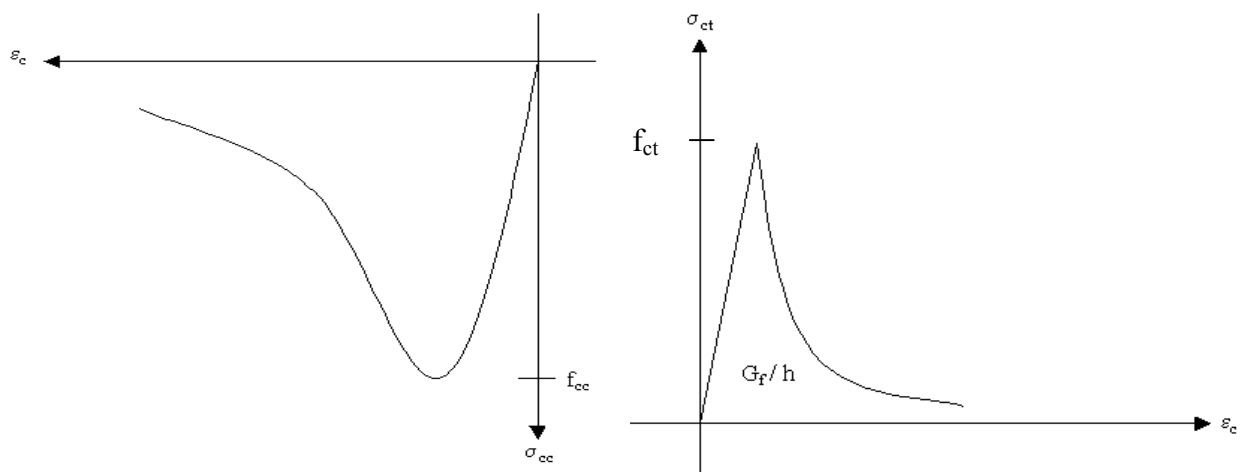


Figure 3.11 a) Stress strain relationship used for concrete in compression, Thorenfeldt. b) Stress strain/crack opening relationship used for concrete in tension, Hordijk.

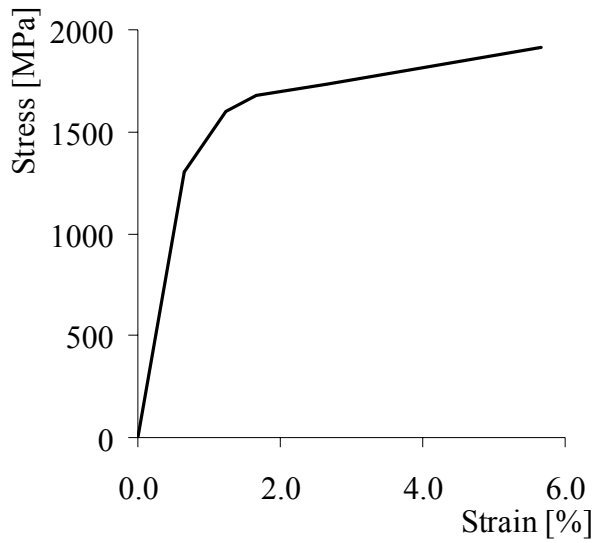


Figure 3.12 Stress strain relationship used for prestressing steel, from tensile tests by Pajari (2003b).

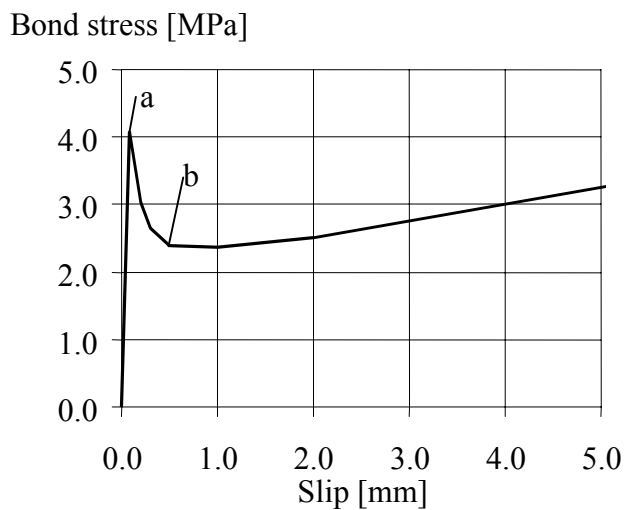


Figure 3.13 Bond-slip relationship used between seven-wire strand and concrete, from pull-through tests by Lundgren (2002). To point a the bond stress increases linear with the slip, between point a and b the bond stress decreases and after point b it slowly increases again, compare with Figure 4.2 and Figure 4.16.

Table 3.2 Material properties used in the analyses of the tests carried out at VTT.

	ST200	ST400/ SF400	STS200	PT200	PT400
Mean concrete compression strength f_{ccm} [MPa]	56.4	52.4	64.9	55.6	57.4
Mean concrete tensile strength f_{ctm} [MPa]	3.57	3.42	3.88	3.54	3.61
Fracture energy G_F [Nm/m ²]	100.7	95.6	111.0	99.7	101.9
Young's modulus of concrete E_{ci} [GPa]	38.3	37.3	40.1	38.1	38.5
Tensile strength of prestressing steel $f_{0.1u}/f_{pu}$ [MPa]	1680/1910	1680/1910	1680/1910	1680/1910	1680/1910
Young's modulus of prestressing steel E_p [GPa]	198	198	198	198	198

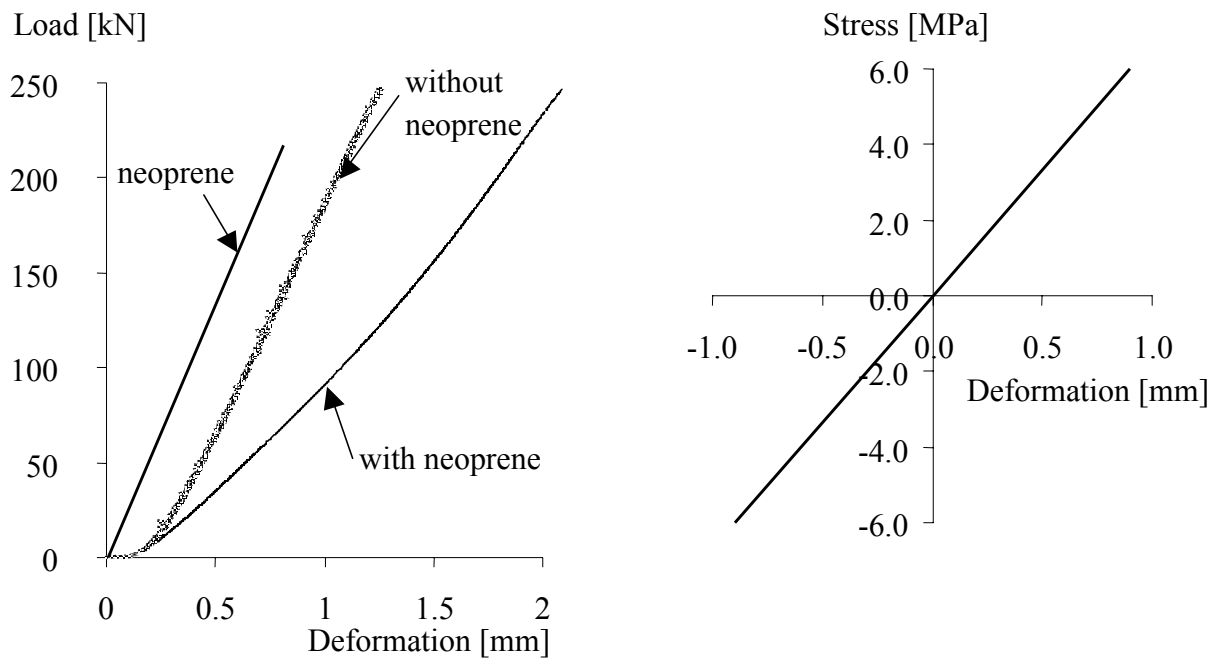


Figure 3.14 a) Evaluation of the stiffness of the neoprene bearing strip. b) Stiffness of the neoprene strip used in analyses, $K = 6.7$ GPa/m.

4 Comparison of Tests and Analyses

4.1 Analyses of shear tension tests on the 200 mm thick units.

Comparison of results from the tests and the analyses on the 200 mm thick hollow core units are shown in Figure 4.1-4.14. As can be seen the overall behaviour, crack pattern and maximum obtained load, is quite well described. Especially for the centrally loaded specimens, the agreement was good. All of the analyses showed the same failure mode as in the tests. However, for the eccentrically loaded hollow core units the maximum load was overestimated. The reason for this is most likely that the torsional stiffness of the beam elements used in the model was too high.

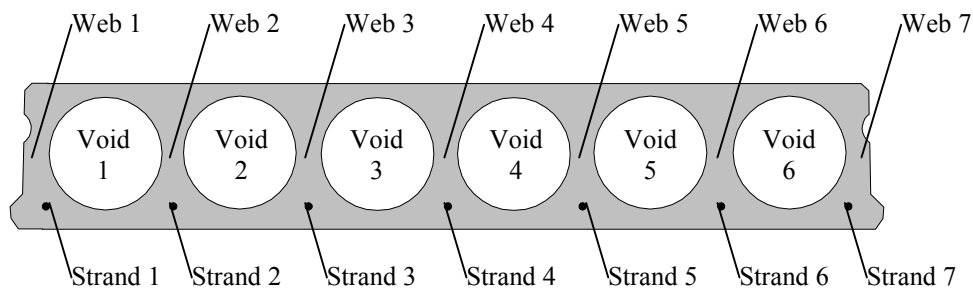


Figure 4.1 Notations used to describe the tests and analyses of the 200 mm thick hollow core slab. Section seen from active end.

In the analyses no adjustment of the initial prestress was made to account for relaxation, creep or shrinkage. The initial prestress for the 200 mm thick hollow core units was 900 MPa. After release of the prestressing force the resulting steel stress in the analyses was 855 MPa and the strands were fully anchored within approximately 0.8 m as can be seen in Figure 4.2. The increase of the steel stress differs slightly between different parts along the length of the strands due to the given bond-slip relationship. Between 0.6 m and 0.8 m the slip of the strands are within the linear branch of the bond-slip curve, see Figure 3.13, between 0.4 m and 0.6 m the slips are within the decreasing branch and from the end section to 0.4 m the slips are larger than in the point where the bond stresses slowly increases again. On the tested specimens there was a large scatter in the measured end slips, from 0.2 mm to 1.9 mm. The corresponding value from the analysis was 1.84 mm, which is within the scatter. In Figure 4.3, the calculated relationship between steel stress and strand slip in the end section at release of the prestressing force is compared with the measured scatter.

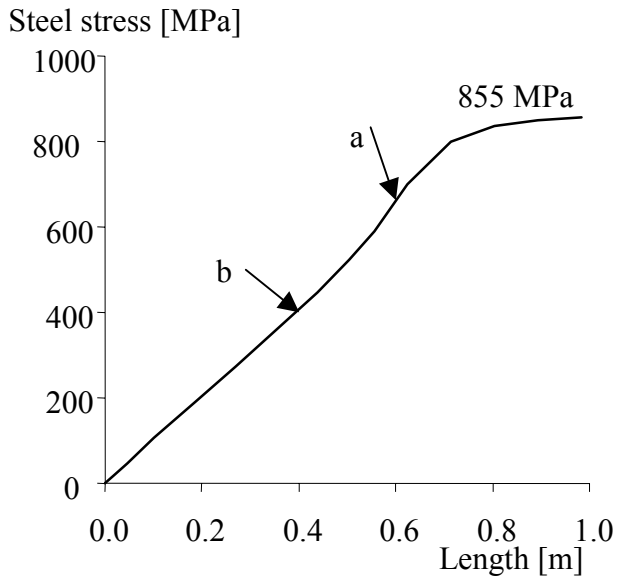


Figure 4.2 Steel stress in strands after release of the prestressing force, result from the analyses on the 200 mm thick hollow core units. Point a and b could be compared with Figure 3.13.

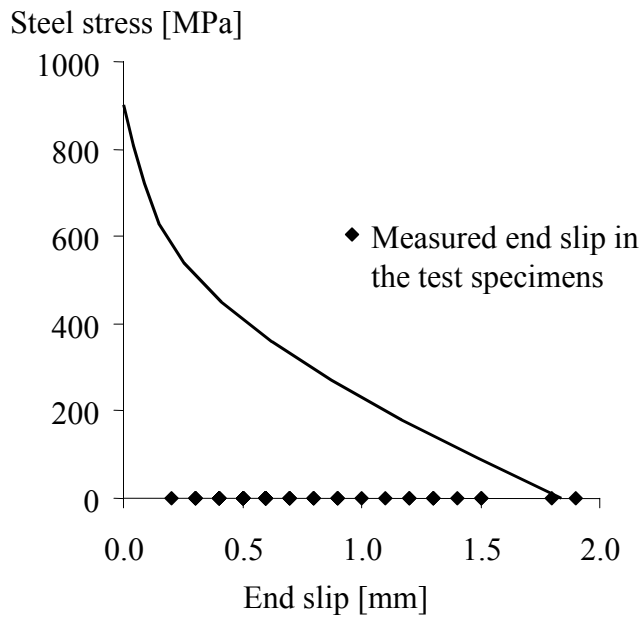


Figure 4.3 Relationship between steel stress and strand slip in the end section at release of the prestressing force. Result from the analyses compared with the range of measured end slips in the 200 mm thick test specimens.

4.1.1 Analysis of the test ST200C

The load versus vertical displacement from the test and the analysis of the centrally loaded hollow core unit, ST200C, is shown in Figure 4.4. In the test the first cracking occurred at $Q = 124$ kN in form of vertical cracks above and below the fifth void. These cracks could not be captured in the analysis of the test. In the test, shear cracks appeared in the third to sixth webs at a maximum load of $Q = 135$ kN. The crack pattern on the tested specimen is shown in Figure 4.5.

In the analysis first shear tension cracks arose in the third to fifth webs at a load of $Q = 120$ kN; then also in the second and the sixth webs at a load of $Q = 123.9$ kN. At the maximum load, $Q = 128.8$ kN, the second to the sixth webs has failed in shear tension and a bending crack arose in the bottom flange of the hollow core unit just under the loads. After the maximum load shear cracks arose also in the outermost webs. The crack pattern from the analysis can be seen in Figure 4.6.

At loading, the strands in the analyses started to slip immediately, see Figure 4.7. This could be explained by the fact that the bond-slip relationship used in the model does not take the pressure from the support action into account. At maximum load, $Q = 128.8$ kN, the slip increased and shear cracks arose in the middle webs. In the test, ST200C; the strands started to slip first after vertical cracks occurred above and below the fifth void at a load of $Q = 124$ kN.

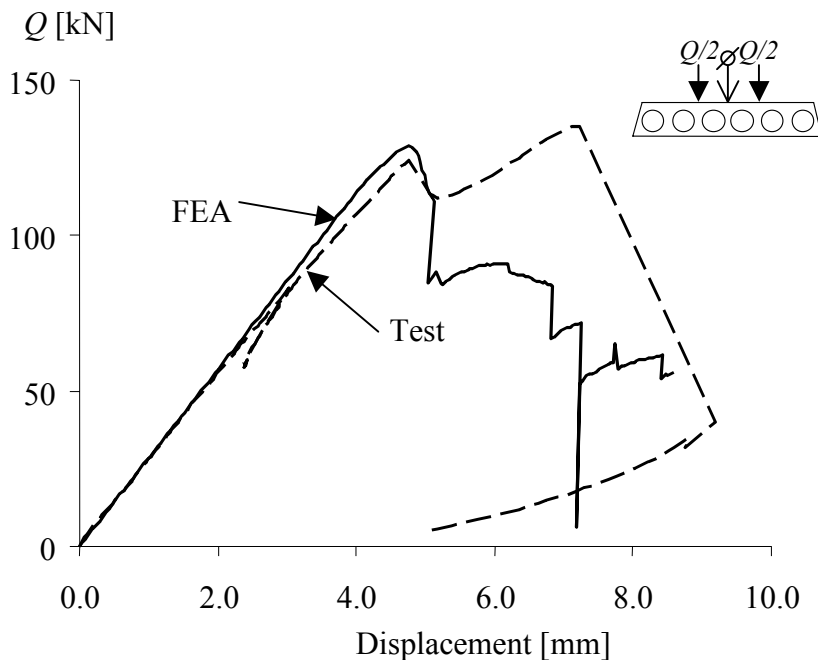


Figure 4.4 Comparison of results from the test and the analysis of ST200C; load versus vertical displacement.



Figure 4.5 Crack pattern from the test ST200C.

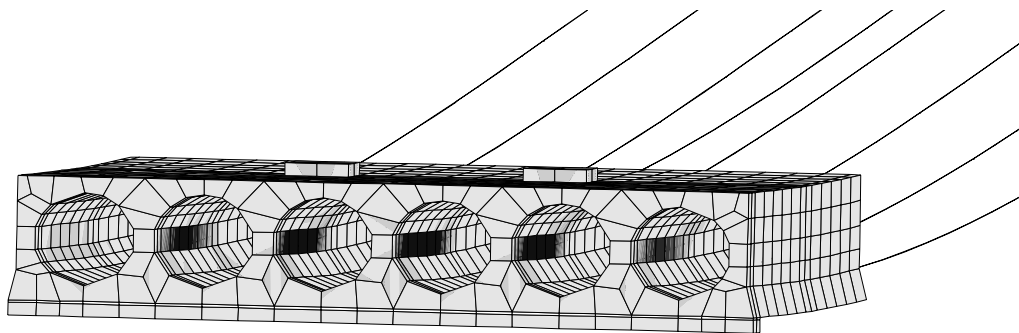


Figure 4.6 Crack pattern from the analysis of ST200C at a load of $Q = 123.9$ kN.

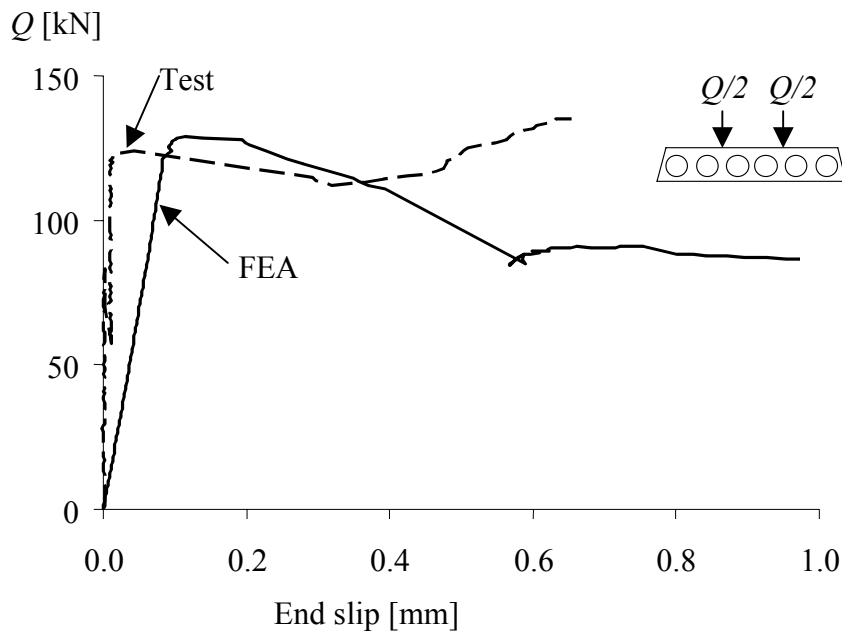


Figure 4.7 Comparison of result from the test and the analysis of ST200C; load versus end slip of strands.

4.1.2 Analysis of the tests ST200E1 and ST200E1b

The load versus vertical displacement from the tests and the analysis of the eccentrically loaded hollow core units, ST200E1 and ST200E1b, is shown in Figure 4.8. In the tests the first cracking occurred at a load of $Q = 95$ kN and $Q = 92$ kN respectively, in form of longitudinal cracks above the sixth void. This crack could not be captured in the analysis of the tests. In the tests, a diagonal crack occurred in the seventh web at a load of $Q = 95,5$ kN and $Q = 92$ kN, respectively. At the maximum load, $Q = 100$ kN and $Q = 98$ kN respectively, a horizontal crack occurred in the seventh web and shear tension cracks occurred in the fifth and sixth webs, and in the fourth to sixth webs respectively. The crack patterns on one of the tested specimens are shown in Figure 4.9.

In the analysis shear tension cracks first arose in the fifth and sixth webs at a load of $Q = 110$ kN then also in the third and the fourth webs. At the maximum load, $Q = 124.4$ kN, there was shear tension cracks in the third to the sixth webs. After the maximum load, a shear crack also arose in the outermost web and a bending crack arose in the bottom flange of the hollow core unit just under the loads. The crack pattern from the analysis can be seen in Figure 4.10.

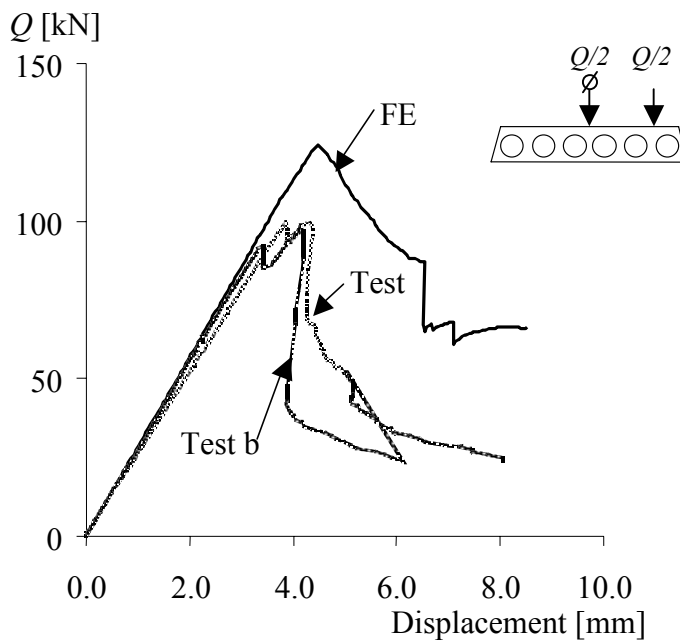


Figure 4.8 Comparison of result from the tests and the analysis for ST200E1 and ST200E1b; load versus vertical displacement.



Figure 4.9 Crack pattern from the test ST200E1.

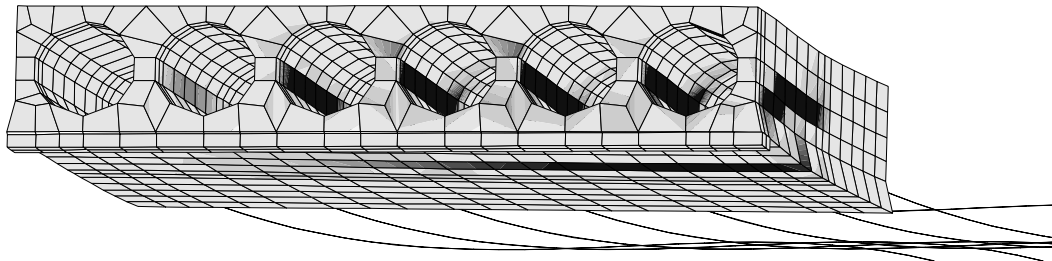


Figure 4.10 Crack pattern from the analysis of ST200E1 at the maximum load, $Q = 124.4$ kN.

4.1.3 Analysis of the test ST200E2

The load versus vertical displacement from the test and the analysis of the eccentrically loaded hollow core unit, ST200E2, is shown in Figure 4.11. In the test the first cracking occurred at $Q = 45$ kN in form of a diagonal crack in the seventh web and longitudinal cracks above and below the sixth void. At a load of $Q = 58$ kN, a horizontal crack occurred in the seventh web. Neither of these cracks could be captured in the analysis of the test. At the maximum load in the test, $Q = 64$ kN, a shear tension crack in the sixth web and a crack in the bottom of the fifth void occurred. The crack pattern on the tested specimen is shown in Figure 4.12.

In the analysis of the test the cracking started with shear tension cracks in sixth and seventh webs at a load of $Q = 95.4$ kN. Then the load decreased and a shear crack arose in the fifth web. The load then increased again, and at $Q = 93.2$ kN a shear tension crack also arose in the fourth web. The maximum load obtained in the analysis was $Q = 104.5$ kN. The crack pattern from the analysis can be seen in Figure 4.13.

In Figure 4.14 the vertical displacements from the test and the analysis in various points across the cross-section are compared. As can be seen, there are rather large differences between the calculated and the observed displacements. The differences are probably due to an overestimated torsional stiffness in the model. This could

depend on the tying between the solid elements and the beam elements. However, most likely it depends on that the torsional stiffness of the beam elements is overestimated. The reason for the overestimation of the torsional stiffness of the beam elements is an error in the used code. As a consequence also the maximum load is overestimated in the analysis.

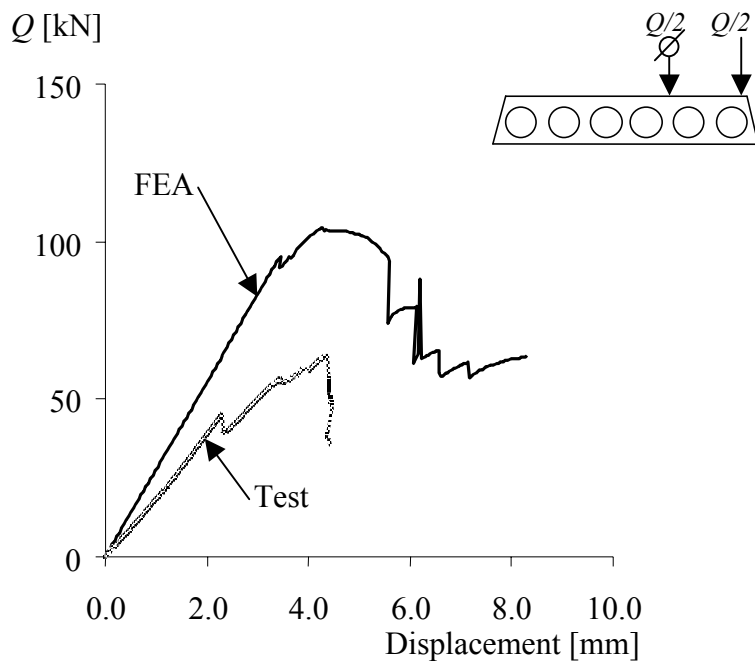


Figure 4.11 Comparison of result from the test and the analysis for ST200E2; load versus vertical displacement.



Figure 4.12 Crack pattern from the test ST200E2.

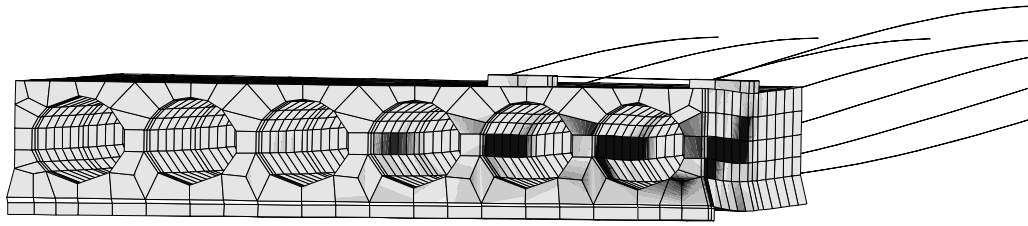


Figure 4.13 Crack pattern from the analysis of ST200E2, at a load of $Q = 93.2$ kN.

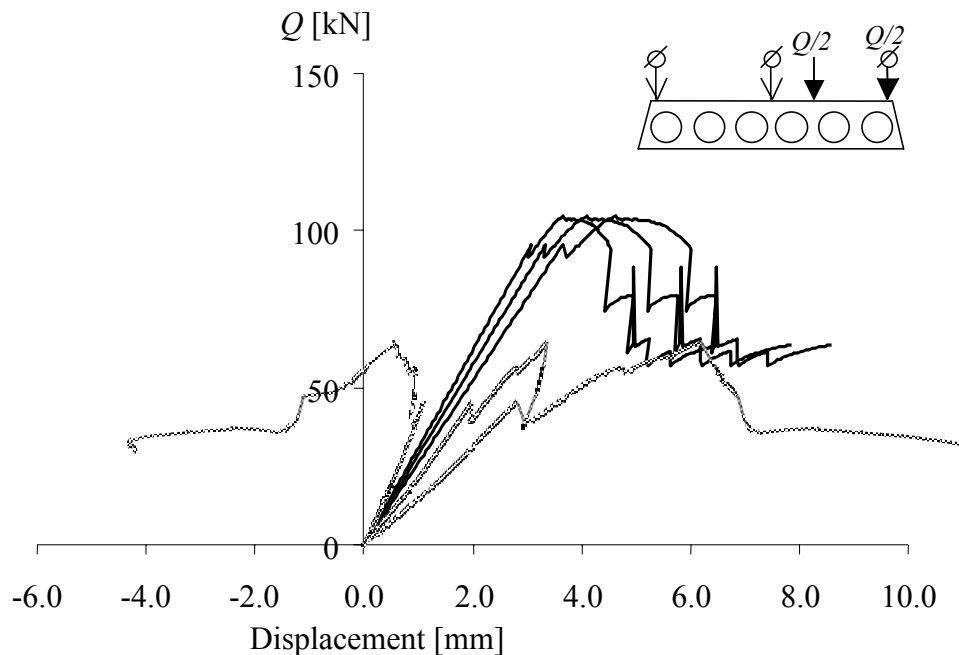


Figure 4.14 Comparison of result from the test and the analysis for ST200E2; load versus vertical displacement.

4.2 Analyses of shear tension tests on the 400 mm thick units

Comparison of results from the tests and the analyses for the tests on the 400 mm thick hollow core units are shown in Figure 4.15-4.29. As can be seen, the finite element analyses were able to capture the overall behaviour, crack pattern and maximum obtained load, with a reasonably good agreement. Especially for the centrally loaded specimens the agreement was good. All of the analyses showed the same failure mode; shear tension failure, as in the tests. However, for the eccentrically loaded hollow core units the maximum load was overestimated. The reason for this is most likely that the torsional stiffness of the beam element used in the model was too high.

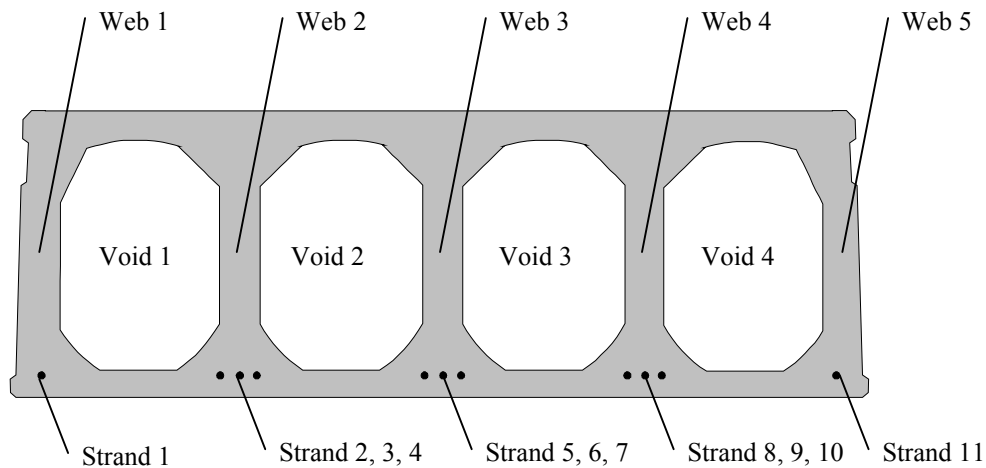


Figure 4.15 Notations used to describe the tests and analyses of the 400 mm thick hollow core slab. Section seen from active end.

In the analyses, no adjustment of the initial prestress was made to account for relaxation, creep or shrinkage. The initial prestress for the 400 mm thick hollow core units was 1000 MPa. After release of the prestressing force the resulting steel stress in the analyses was 946 MPa and the strands were fully anchored within approximately 0.9 m as can be seen in Figure 4.16. On the tested specimen there was a large scatter in the measured end slips, from 0.6 mm to 2.7 mm. The corresponding value from the analysis was 2.26 mm, which is within the scatter. In Figure 4.17, the calculated relationship between steel stress and strand slip in the end section at release of the prestressing force is compared with the measured scatter.

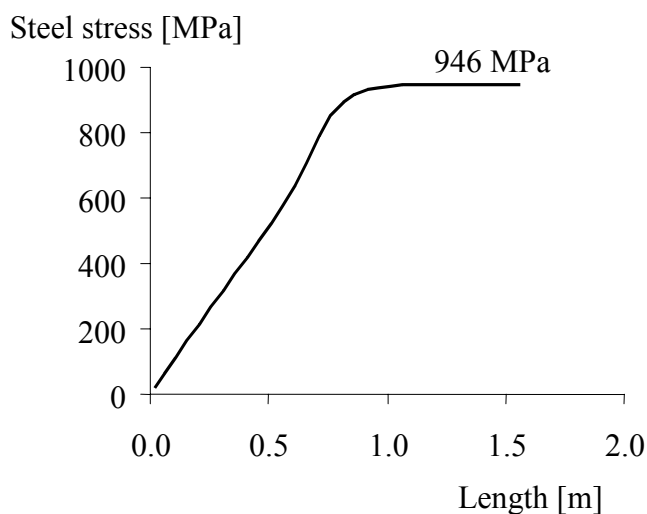


Figure 4.16 Steel stress in strands after release of the prestressing force, result from the analyses on the 400 mm thick hollow core units.

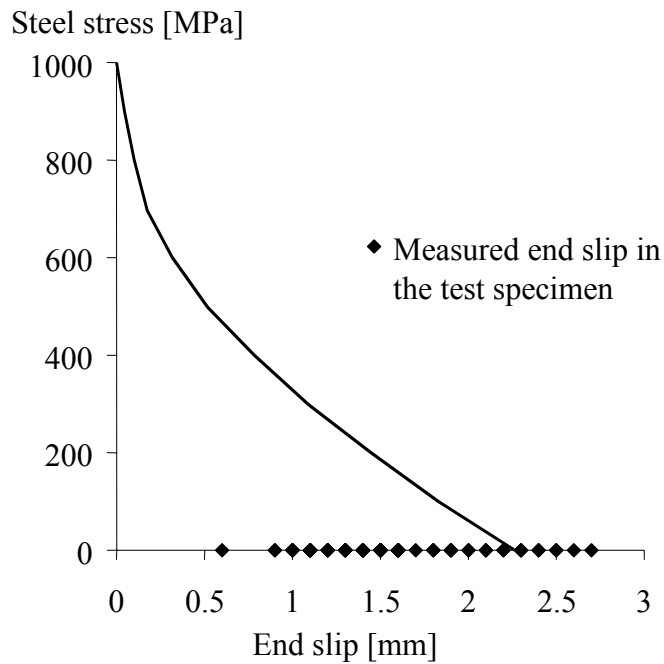


Figure 4.17 Relationship between steel stress and strand slip in the end section at release of the prestressing force. Result from the analyses compared with the range of measured end slips in the 400 mm thick tests specimens.

4.2.1 Analysis of the test ST400C

The load versus vertical displacement from the test and the analysis of the centrally loaded hollow core unit, ST400C, is shown in Figure 4.18. In the test the first cracking occurred at a load of $Q = 211$ kN in form of a diagonal crack in the fifth web. At a load of $Q = 218$ kN, longitudinal cracks occurred above and below the fourth void. At the maximum load, $Q = 258$ kN, shear tension cracks in the third and fourth webs and longitudinal cracks above and below the third void occurred. The crack pattern on the tested specimen is shown in Figure 4.19.

In the analysis, the first cracking arose at the maximum load $Q = 247$ kN in form of a shear tension crack in the third web and a longitudinal crack in the bottom of the second web. After the maximum load, shear tension cracks in the second, fourth, and fifth webs, and a longitudinal crack in the bottom of the first void arose. The crack pattern from the analysis can be seen in Figure 4.20.

In the test, ST400C, the sixth strand started to slip at a load of approximately 50 kN and at maximum load ($Q = 258$ kN) the sixth strand has slipped 2.5 mm as shown in Figure 4.21. The neighbouring strands in the same web started to slip at a load of approximately 110 kN and 150 kN, and at maximum load they had slipped 1.0 mm and 0.5 mm. All other strands started to slip at maximum load. The large slips of strand 5-6 were not captured in the analysis. At loading, the strands in the analyses started to slip immediately, see Figure 4.21. This could be explained by the fact that the bond-slip relationship used in the model does not take the pressure from the

support action into account. At maximum load, $Q = 247$ kN, the slip increased when shear cracks arose in the middle webs.

The measured displacements over the cross-section, at each web, shows that the hollow core unit bends also in the transversal direction, see Figure 4.22. These displacements are smaller in the analysis. One possible explanation is the longitudinal cracks, in the top and the bottom flange of the hollow core unit, which occurs in the tests but not in the analyses. Another explanation could be the course mesh that is less accurate in describing bending.

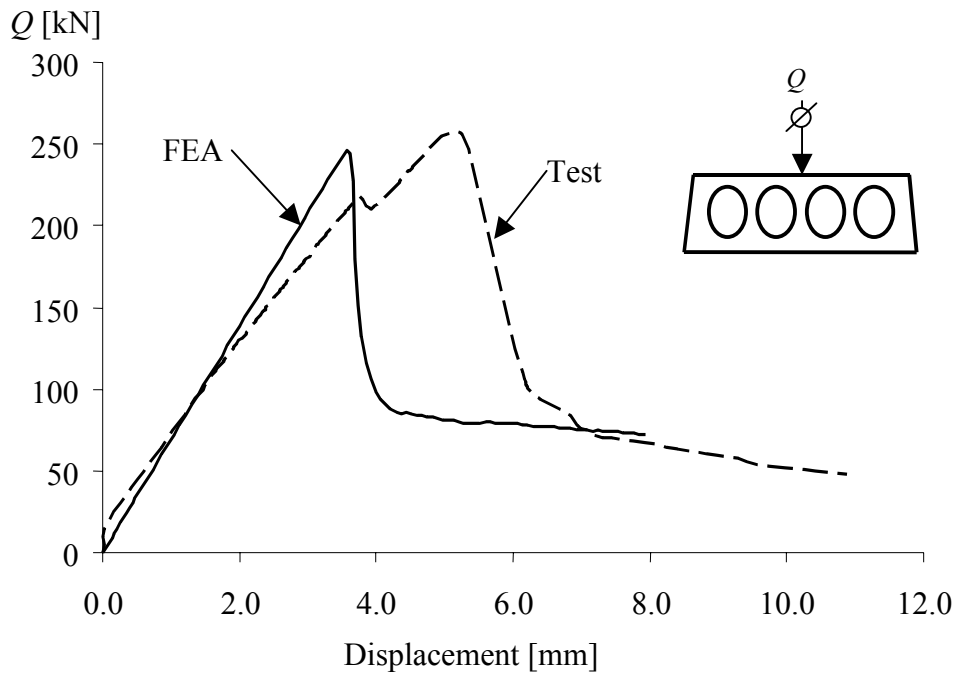


Figure 4.18 Comparison of result from the test and the analysis for ST400C; load versus vertical displacement.

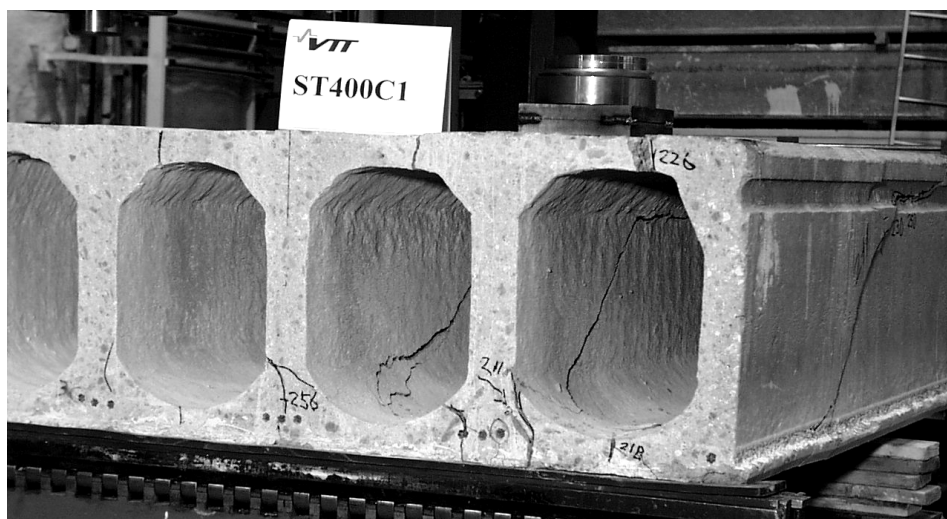


Figure 4.19 Crack pattern from the test ST400C.

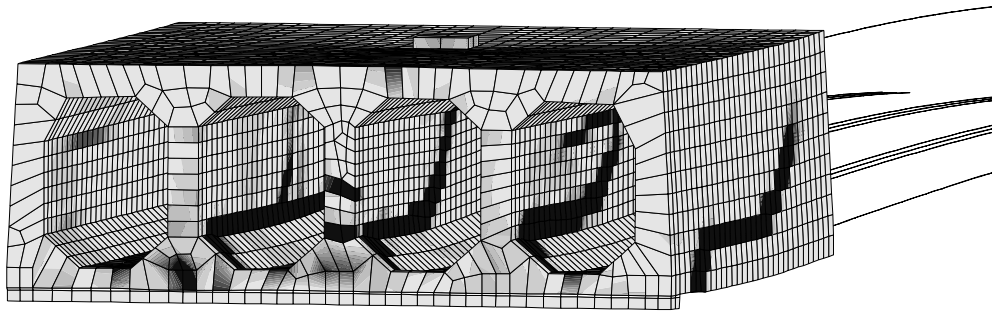


Figure 4.20 Crack pattern from the analysis of ST400C, after maximum load.

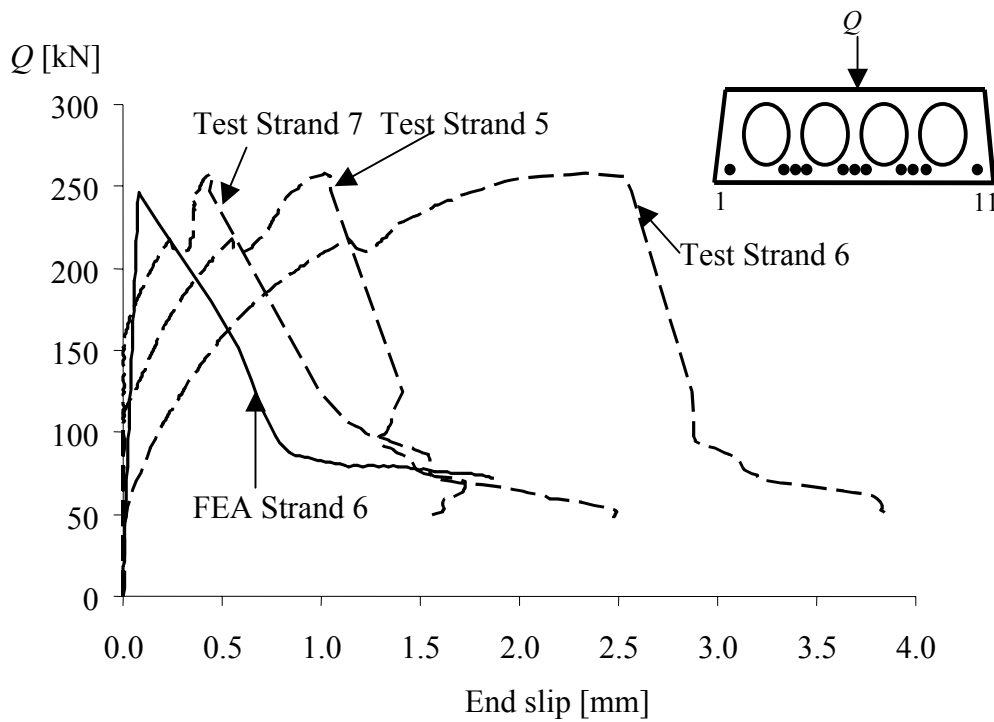


Figure 4.21 Comparison of result from the test and the analysis for ST400C; load versus end slip of strands.

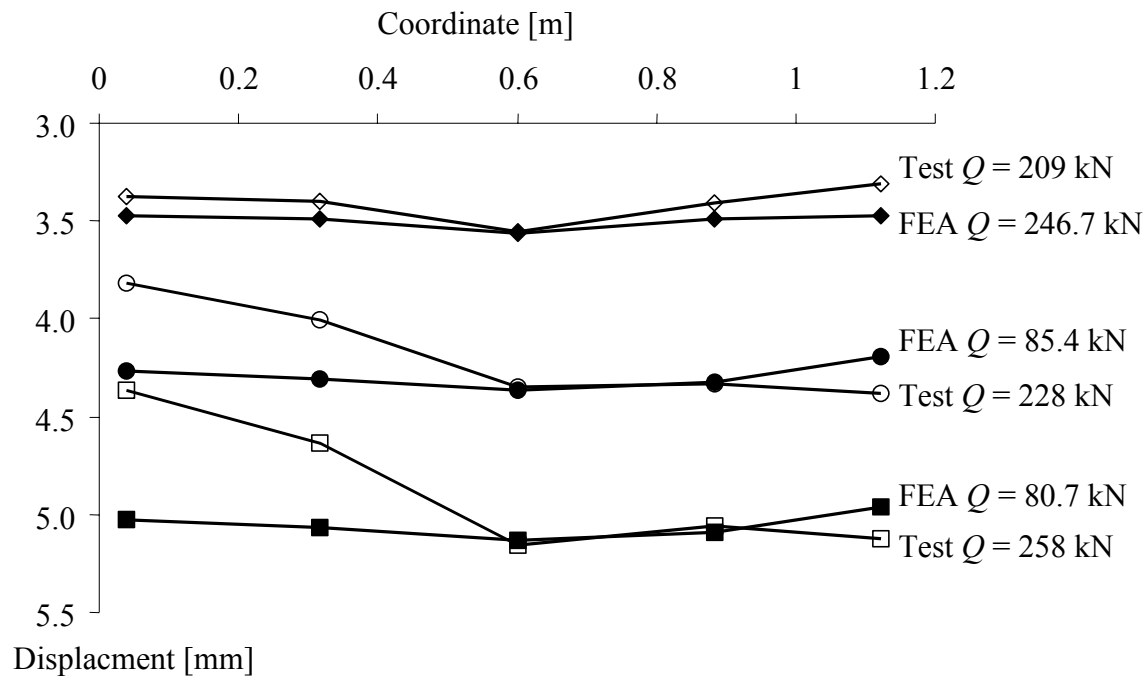


Figure 4.22 Comparison of result from the test and the analysis for ST400C; displacement measured over the cross-section at each web.

4.2.2 Analysis of the test ST400C2

The load versus vertical displacement for the test and the analysis of the centrically loaded hollow core unit, ST400C2, is shown in Figure 4.23. In the test, the first cracking occurred at a load of $Q = 145$ kN in form of a longitudinal crack over the first void. At a load of $Q = 193$ kN, a diagonal crack in the first web and a longitudinal crack below the first void occurred. A horizontal crack in the first web occurred at a load of $Q = 220$ kN. At the maximum load, $Q = 272$ kN, shear tension cracks in the second to fifth webs occurred. The crack pattern on the tested specimen is shown in Figure 4.24.

In the analysis, the first cracking arose at the maximum load $Q = 300.8$ kN in form of shear tension cracks in the second to fourth webs and a longitudinal crack in the bottom of the first void. After the maximum load shear tension cracks in the first and fifth webs and longitudinal cracks above the first and fourth void arose. The crack pattern from the analysis can be seen in Figure 4.25.

As can be seen in Figure 4.27, the strands started to slip in the test at the maximum load. The strands in the analysis started to slip immediately at loading as explained before, see Chapter 4.2.1. The slip of the strands in the analysis increased after maximum load.

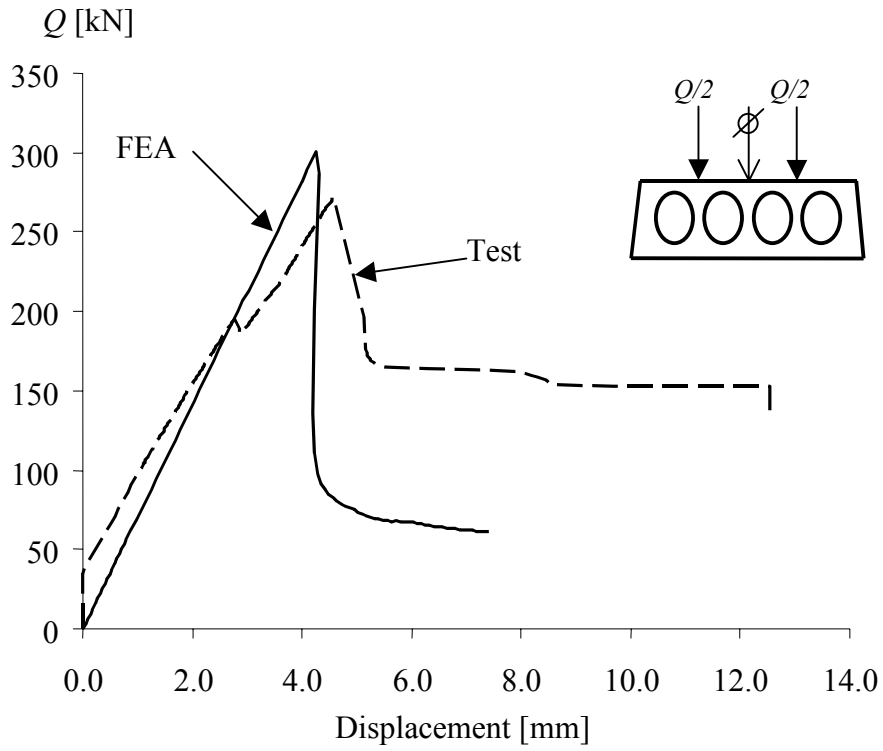


Figure 4.23 Comparison of result from the test and the analysis for ST400C2; load versus vertical displacement.



Figure 4.24 Crack pattern from the test ST400C2.

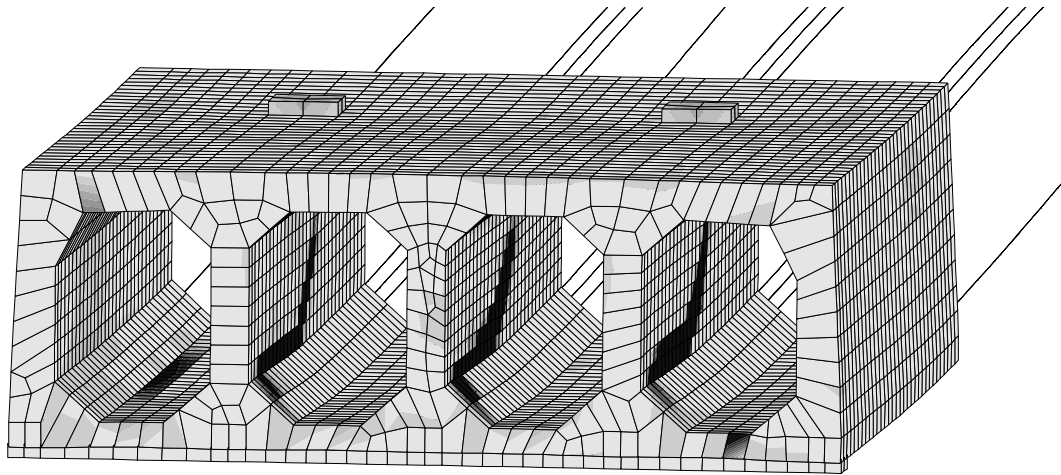


Figure 4.25 Crack pattern from the analysis of ST4002C, at maximum load $Q = 300.8 \text{ kN}$.

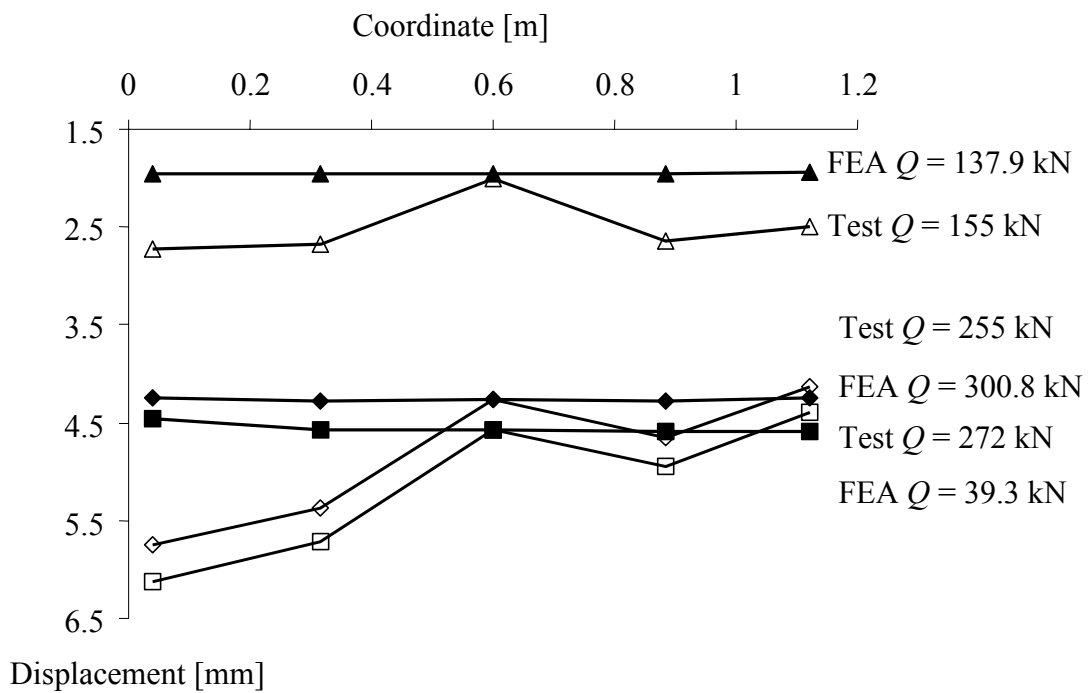


Figure 4.26 Comparison of result from the test and the analysis for ST400C2; displacement measured over the cross-section at each web.

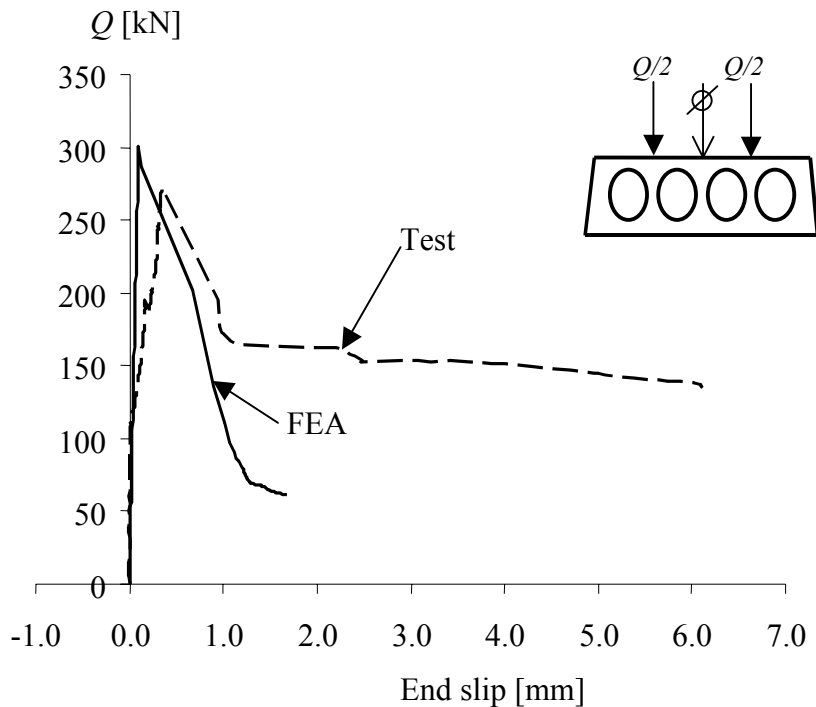


Figure 4.27 Comparison of result from the test and the analysis for ST400C2; load versus end slip of strand Nr: 3.

4.2.3 Analysis of the test ST400E1

The load versus vertical displacement for the test and the analysis of the eccentrically loaded hollow core unit, ST400E1, is shown in Figure 4.28. In the test the first cracking occurred at a load of $Q = 148$ kN in form of a diagonal crack in the fifth web. At a load of $Q = 150$ kN, a longitudinal crack below the fourth void occurred. At the maximum load, $Q = 167$ kN, a shear tension crack and a horizontal crack occurred in the fourth web, and an almost vertical crack about 3 cm from the edge occurred in the third web. The crack pattern on the tested specimen is shown in Figure 4.29.

In the analysis, the first cracking arose at the maximum load, $Q = 239$ kN, in form of shear tension crack in the fourth web and a longitudinal crack in the bottom of the third web. After the maximum load, shear tension cracks in the second web, and longitudinal cracks above and below the fourth void arose. The crack pattern from the analysis can be seen in Figure 4.30.

In Figure 4.31, the vertical displacement from the test and the analysis on various positions across the cross-section are compared. As can be seen, there are, as well as for the test ST200E2, rather large differences between the calculated and the observed displacements. This is most likely explained by the overestimated torsional stiffness of the beam elements, see Chapter 4.1.3. As a consequence also the maximum load is overestimated in the analysis.

As can be seen in Figure 4.33, the strands started to slip in the test at a load of $Q = 148$ kN, when the first crack occurred. After maximum load the slip increased. The strands in the analysis started to slip immediately at loading as explained before, see Chapter 4.2.1. The slip of the strands in the analysis increased after maximum load.

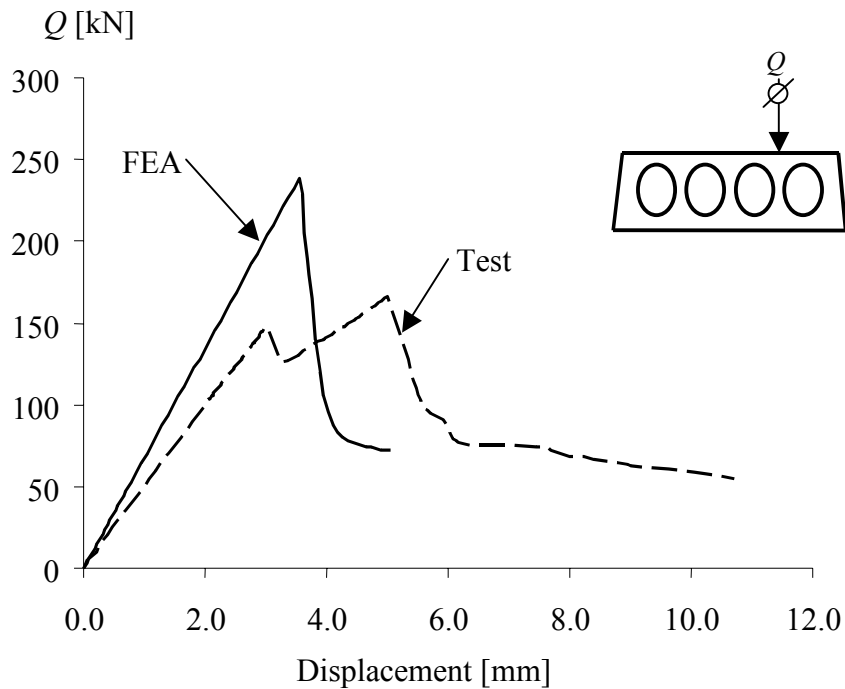


Figure 4.28 Comparison of result from the test and the analysis for ST400E1; load versus vertical displacement.



Figure 4.29 Crack pattern from the test ST400E1.

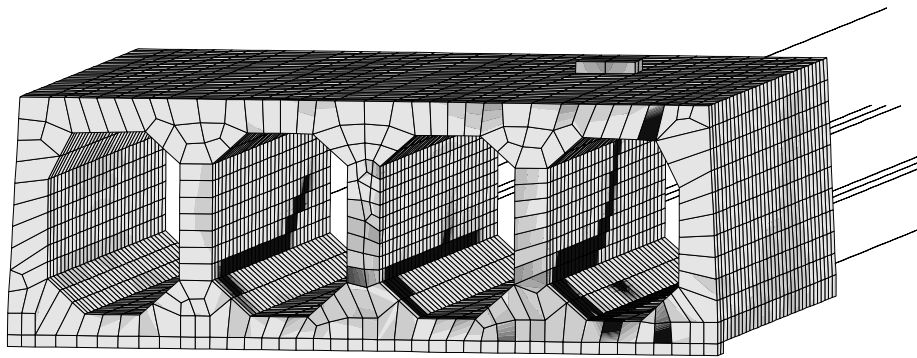


Figure 4.30 Crack pattern from the analysis of ST400E1, after maximum load.

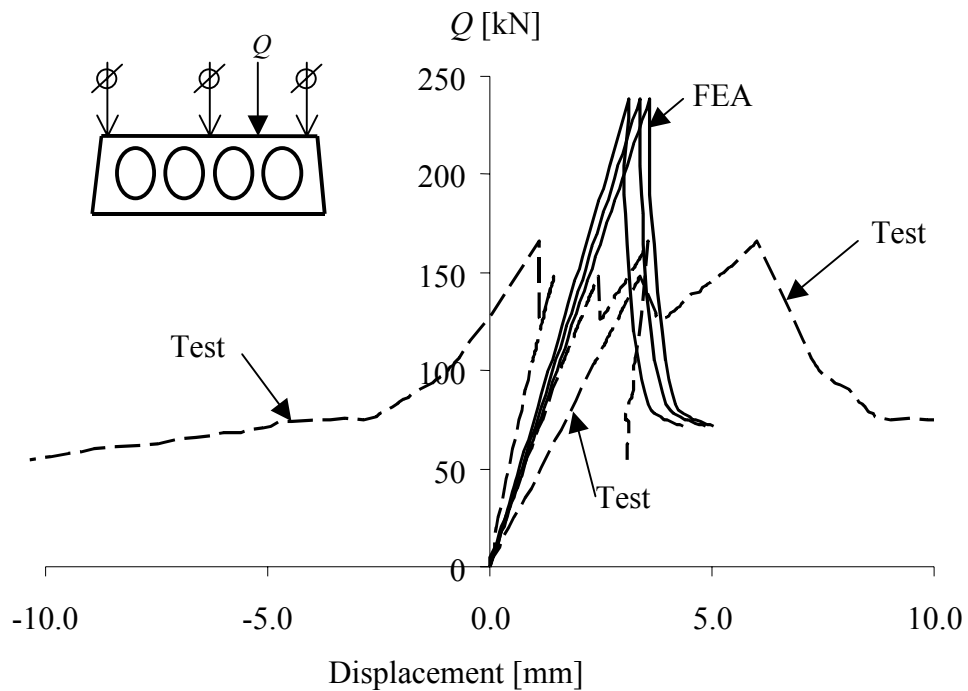


Figure 4.31 Comparison of result from the test and the analysis for ST400E1; load versus vertical displacement.

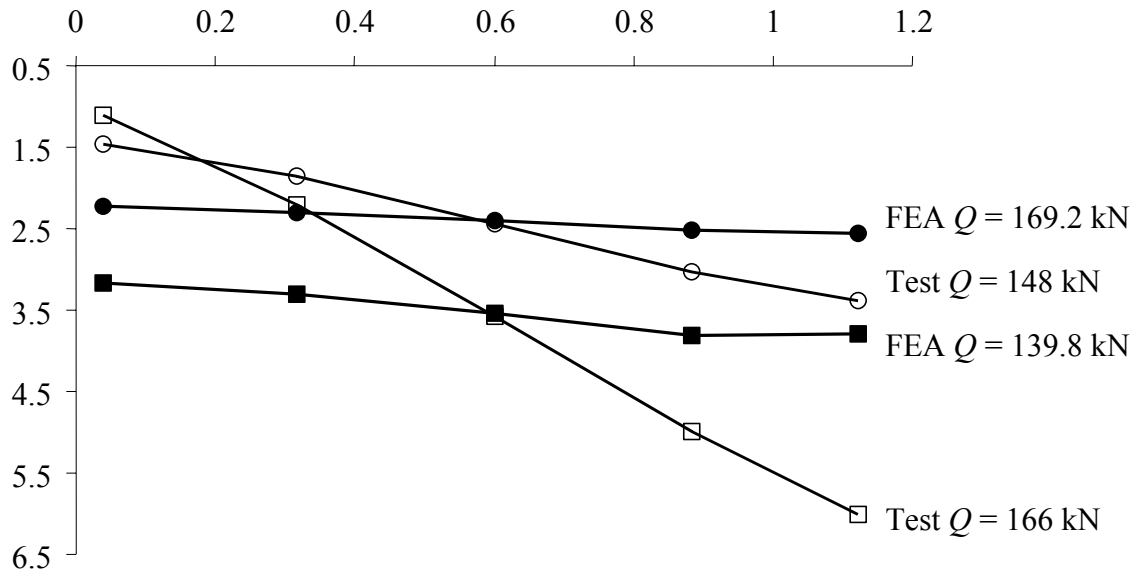


Figure 4.32 Comparison of result from the test and the analysis for ST400E1; displacement measured over the cross-section at each web.

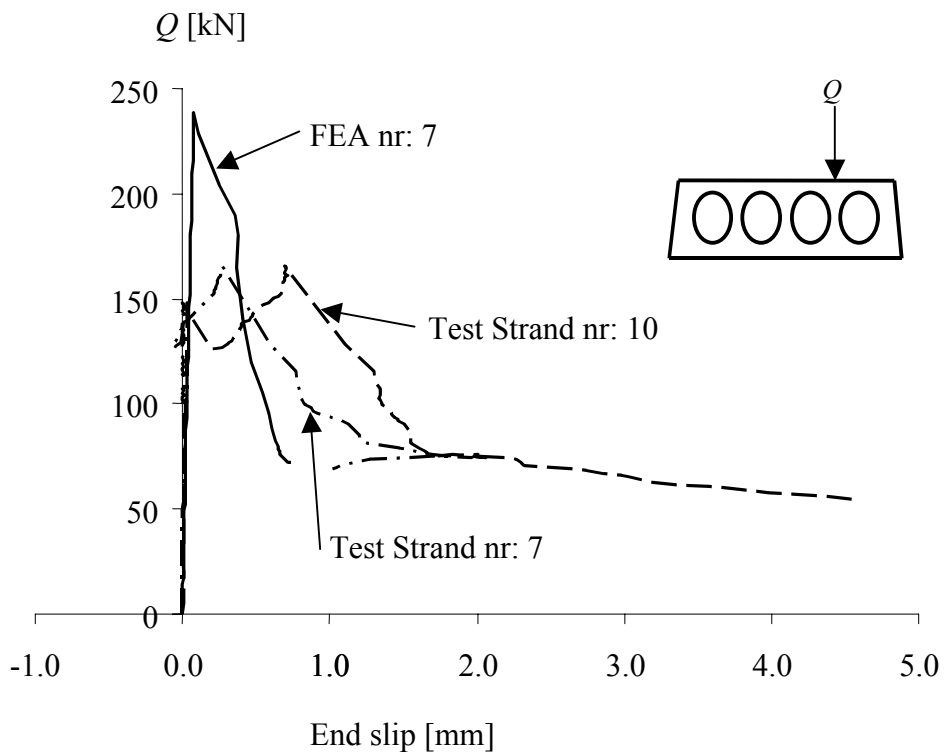


Figure 4.33 Comparison of result from the test and the analysis for ST400E1; load versus end slip of strands.

4.3 Discussion of the analyses of shear tension tests

In Figure 4.34, the evaluated maximum loads are compared to the measured ones for all analysed shear tension tests. As can be seen, there is a rather good agreement. In Figure 4.35, the ratios between the maximum loads in the analyses and in the tests are plotted versus the load eccentricity. There it can be seen that there is a clear tendency in the results, that the larger the load eccentricity, the larger the difference between the maximum loads. For the centrally loaded specimens (load eccentricity in Figure 4.35 is zero), the agreement is very good. However, for the eccentrically loaded hollow core units the maximum load is overestimated. Most likely, this is due to that the torsional stiffness of the beam elements used in the models was too high. One effect of this can also be seen in Figures 4.14, 4.31 and 4.32, where it is clear that there was a rather large difference in the torsional rotation.

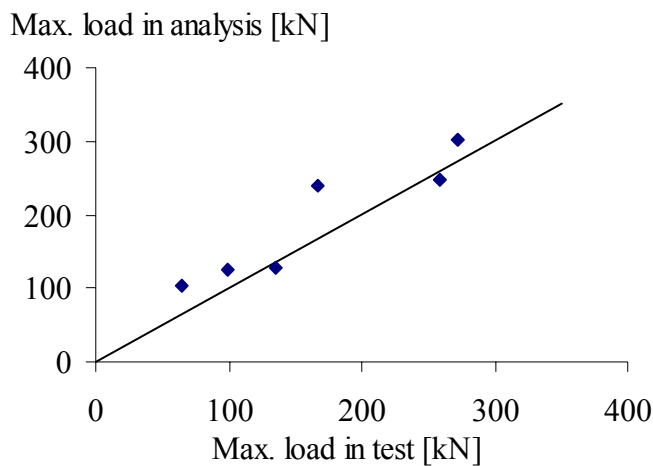


Figure 4.34 Evaluated maximum loads in analyses compared to the measured ones in the shear tension tests by Pajari (2003b).

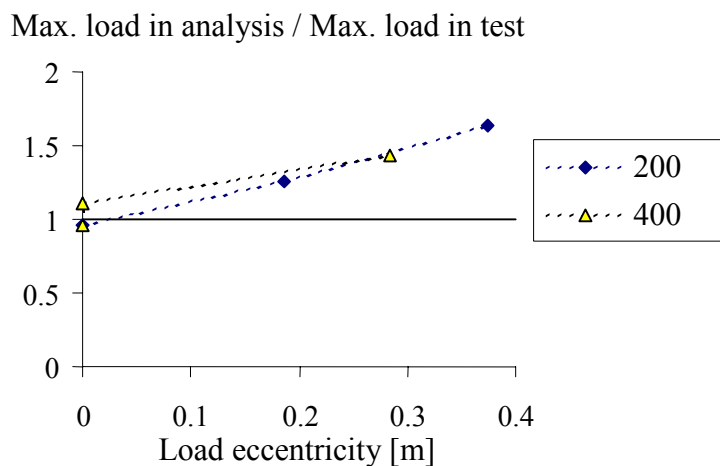


Figure 4.35 Evaluated maximum loads in analyses compared to the measured ones in the shear tension tests by Pajari (2003b).

Another difference between test and analyses results were the longitudinal cracking above and below some of the voids that appeared in several of the shear tension tests. These cracks were not obtained in the analyses. One reason for these cracks might be that they were initiated during production, when the slab units were cut by sawing, see Pajari (2003a). For the 400 mm thick hollow core units, there was also another difference between the test and the analyses results: in all the tests on 400 mm thick hollow core units, the first shear tension crack appeared in one of the outermost webs, while in the analyses, it was always one of the inner webs that cracked first. Again, this difference might be due to weaknesses that were initiated during production, since the outermost webs were compacted only from one side, while the inner webs were compacted from both sides.

4.4 Analyses aiming at shear flexure failure

Within the project, one test aiming at a shear flexure failure was conducted. However, instead of a shear flexure failure, a shear tension failure was obtained, see Pajari (2003b). One analysis of the tested specimen was carried out. Furthermore, some variations in the test set-up were analysed, in order to investigate when a shear flexure failure would be possible to occur. The following analyses were carried out:

1. Specimen tested, initial prestress 1000 MPa
2. The same as 1, but with the load closest to the mid span doubled
3. The same as 1, but with an initial prestress of 600 MPa
4. The same as 1, but without prestress

For these analyses, the main interest was to study the failure mode; the possibility to compare actual loads with the ones in tests was considered as less important. Therefore, only one half of a web was modelled. A symmetry line in the mid span was also used. The finite element mesh used is shown in Figure 4.36.

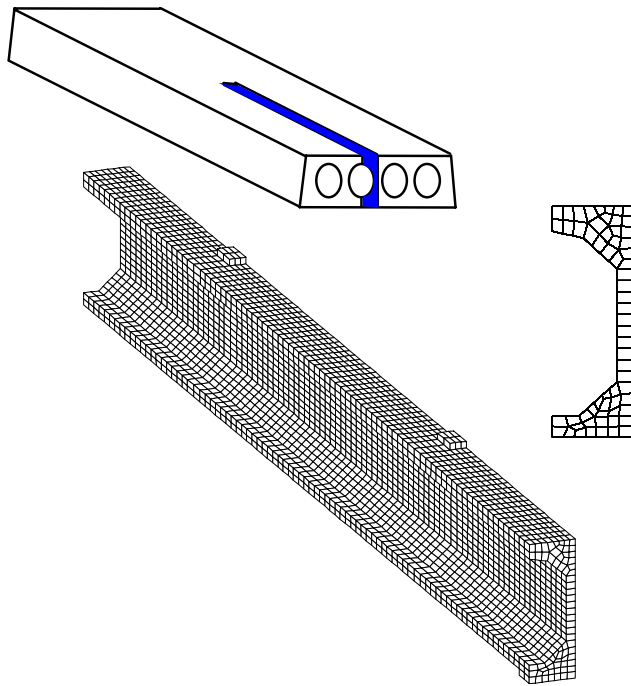


Figure 4.36 The finite element mesh used in the analyses aiming at shear flexure failure.

The crack pattern in the analysis of the tested specimen is shown in Figure 4.37, and the load versus the vertical deformation in the mid span is shown in Figure 4.38. Some important events are marked in this curve; i.e. when different cracks appear, and when the prestressing steel starts yielding. As can be seen, a shear tension crack develops in the support span at the same time as the reinforcement starts yielding. Thereafter, the load increased slightly more, and the maximum load is limited by a failure in the compressive zone at the load closest to the mid span. The failure mode in the analysis is mainly a bending failure, but it must be noted that the shear tension failure is very close. Actually, it can be debated whether it is reasonable that the load can be increased after the shear tension crack has developed. In the model, there are at this point tensile stresses larger than the tensile strength of the concrete that are transferred. Even though the used material model shall limit the tensile stresses to the tensile strength, such transfer of stresses is possible in the model due to an effect that is usually denoted “stress locking”, explained by for example Jirásek (1999). Thus, it can be concluded that a shear tension failure is rather likely to occur in reality. In the analysis the “stress locking” may prevent this failure mode.

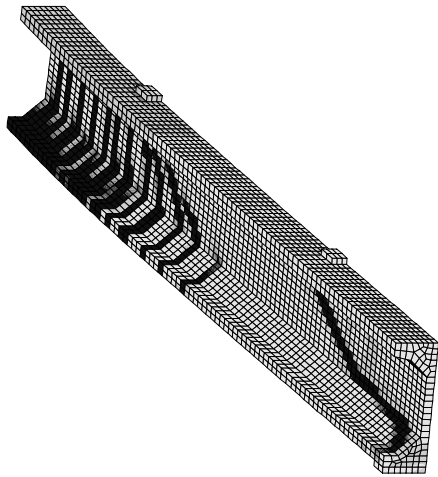


Figure 4.37 Crack pattern in the analysis of the tested specimen at a load of 18.4 kN.

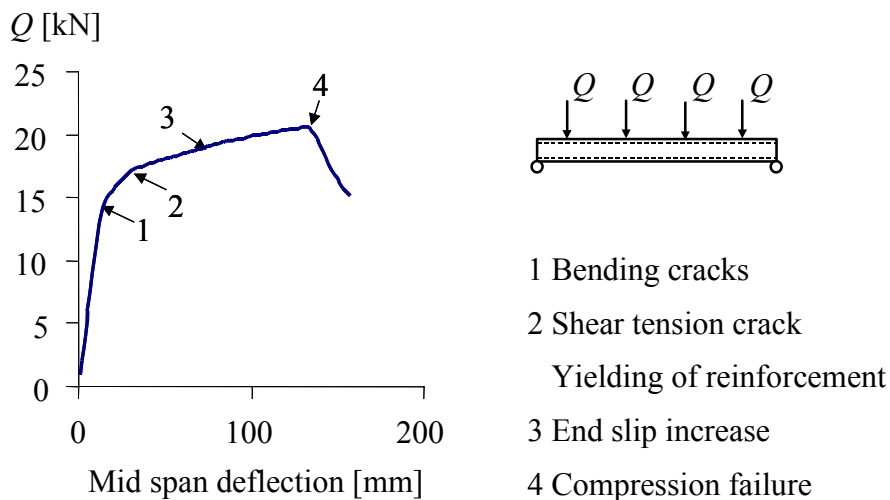


Figure 4.38 The load versus the vertical displacement in mid span obtained in the analysis of the tested specimen.

Since the failure mode in the test carried out was shear tension failure, an analysis was carried out where the load closest to the mid span was doubled, see Figure 4.39. The intention was to increase the shear force in the second span, to provoke a shear flexure failure. The load versus mid span deflection obtained in this analysis is shown in Figure 4.39. As can be seen, shear flexure cracks now form before a shear tension crack appears. The prestressing steel starts yielding before the shear flexure cracks develop. In the analysis, the failure mode is a bending failure. However, in reality a shear flexure failure might occur. It was concluded that in order to obtain a shear flexure failure, using the first test set-up, the prestress had to be decreased. Two cases were investigated; with an initial prestress of 600 MPa, and without prestress. The results are shown in Figures 4.40 – 4.42.

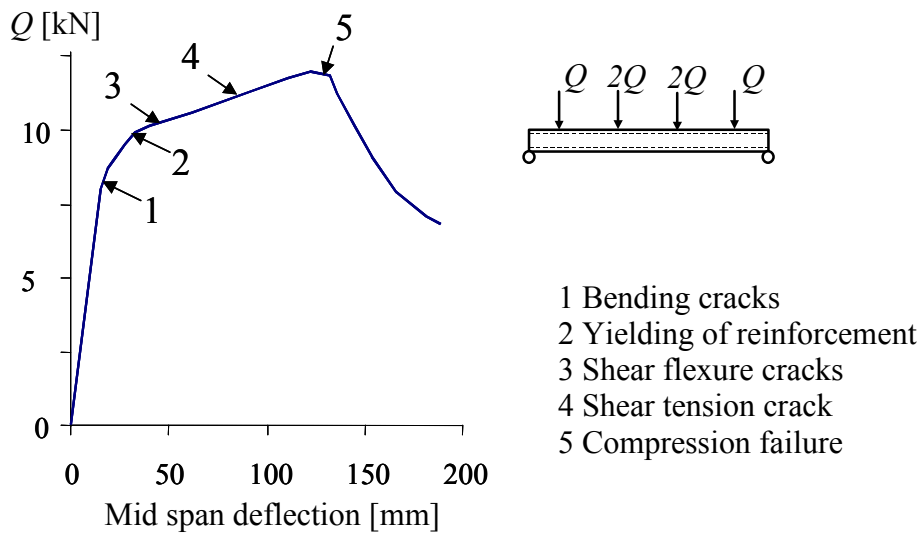


Figure 4.39 The load versus the vertical displacement in mid span obtained in the analyses of a similar specimen as the one tested, but with the load closest to the mid span doubled.

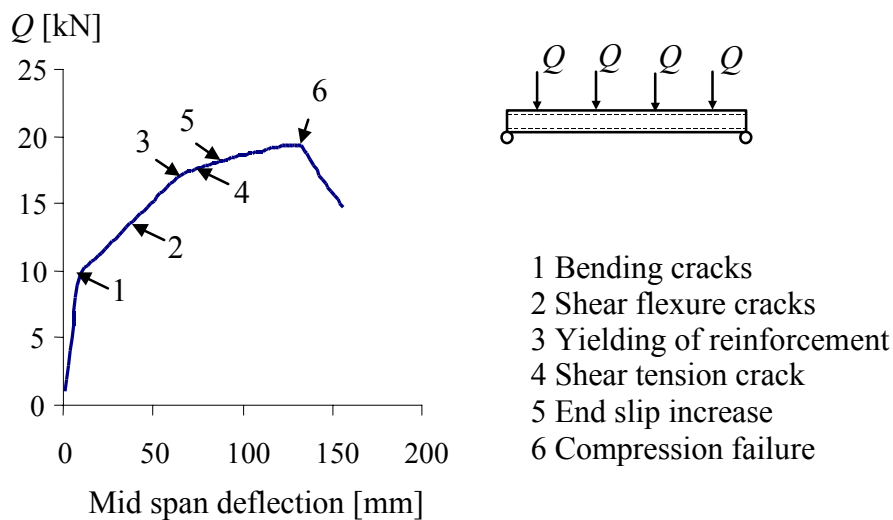


Figure 4.40 The load versus the vertical displacement in mid span obtained in the analyses of a similar specimen as the one tested, but with an initial prestress of 600 MPa instead of 1000 MPa.

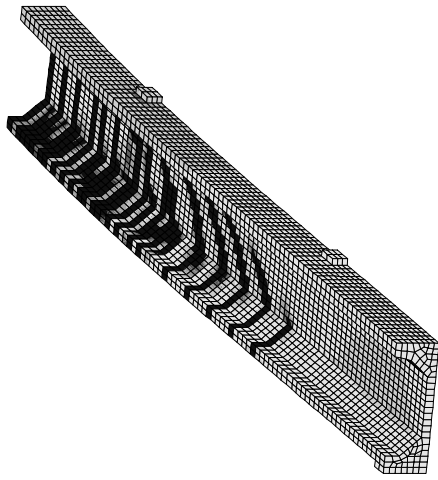


Figure 4.41 Crack pattern in the analysis of a similar specimen as the one tested, but with an initial prestress of 600 MPa, at a load of 17.1 kN.

When the initial prestress was decreased to 600 MPa, shear flexure cracks appeared before the prestressing steel started to yield. It is possible that a shear flexure failure would take place if such a test was carried out. In the analysis, it was possible to increase the load after the appearance of the shear flexure cracks, but large tensile stresses were transferred. The maximum load was obtained when the compressive side fractured. In reality, it is uncertain if it would be possible to increase the load this much after the shear flexure cracks had formed.

To investigate if the shear flexure failure could be described in such analyses, an extreme case was analysed; without any prestress, without softening of the concrete in compression, with elastic reinforcement, and with an increased end anchorage capacity. These choices were done in order to avoid other possible failure modes. The result from this analysis is shown in Figure 4.42. As can be seen, shear flexure cracks then appear for a rather low load. However, they do not lead to failure; instead the load can be increased unlimitedly. This is possible due to the stress locking effect; the transfer of stresses larger than the tensile stress were noted as soon as the shear flexure cracks appeared, and the transferred stresses became larger and larger the higher the applied load was. Already at a load of $Q = 10$ kN the largest tensile stress in the concrete was 14 MPa, to be compared with the assumed tensile strength of 3.42 MPa. It was concluded that the shear flexure failure can not be described in this type of model. However, following the results from the two first types of analyses, it was concluded that a shear flexure failure is rather unlikely to occur for slabs where standard prestress levels are used.

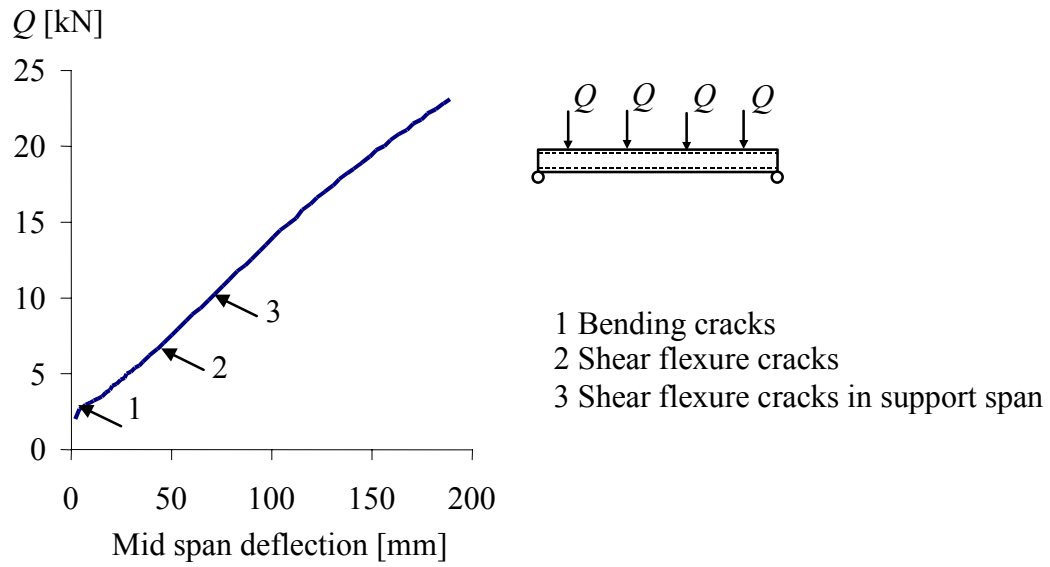


Figure 4.42 The load versus the vertical displacement in mid span obtained in the analyses of a specimen without prestress, with elastic reinforcement and an increased end anchorage capacity.

5 Conclusions

Non-linear finite element analyses of individual hollow core units, subjected to different combinations of shear and torsion, were carried out. Concerning the modelling technique to describe shear and torsion in a single hollow core unit, much was learned. As beam elements are not capable of describing failure due to shear stresses, solid elements have to be used. It was shown that even with a rather coarse mesh, the cracking of the webs at a shear tension failure could be described. However, even when a coarse mesh was used, modelling of a whole slab with solid elements resulted in a very large model and time-consuming analyses. Simplifications of the model are therefore necessary. Here, it was chosen to model only the part of the hollow core unit where the shear tension failure will take place with solid elements. The rest of the hollow core unit was modelled with beam elements. If the response after maximum load is of interest, it was found that the interaction between the prestressing steel and the concrete must be included, for example by using a bond-slip relation.

In general, the finite element analyses of the shear tension tests were able to capture the overall behaviour, failure mode, crack pattern, and maximum obtained load, with a reasonably good agreement. Especially for the centrally loaded specimens, the agreement was good. However, for the eccentrically loaded hollow core units the maximum load was overestimated. Furthermore, there was a rather large difference in the torsional rotation. Most likely, these two results are coupled, and both depend on that the torsional stiffness of the beam elements used in the models was too high.

Another difference between test and analyses results were the longitudinal cracking above and below some of the voids that appeared in several of the shear tension tests. These cracks were not obtained in the analyses. One reason for these cracks might be that they were initiated during production, when the slab units were cut by sawing, see Pajari (2003a). For the 400 mm thick hollow core units, there was also another difference between the test and the analyses results: in all the tests on 400 mm thick hollow core units, the first shear tension crack appeared in one of the outermost webs, while in the analyses, it was always one of the inner webs that cracked first. Again, this difference might be due to weaknesses that were initiated during production, since the outermost webs were compacted only from one side, while the inner webs were compacted from both sides.

Some analyses aiming at a shear flexure failure were also carried out. The aim with these analyses was to search for a loading situation where a shear flexure failure would be critical. In some of the investigated load situations, shear flexure cracks appeared. Yet, due to stress locking in the analyses, large tensile stresses were transferred over the shear flexure cracks, and thus, it was concluded that the shear flexure failure could not be described in the type of model used. However, it was concluded that a shear flexure failure is rather unlikely to occur for slabs where standard prestress levels are used.

6 References

- Byggtjänst. (1994): *Betonghandbok- Material*, AB Svensk Byggtjänst and Cementa AB.
- CEB. (1993): *CEB-FIP Model Code 1990*, Bulletin d'Information 213/214, Lausanne, Switzerland.
- CEB. (1995): *High Performance Concrete, Recommended Extension to the Model Code 90*, Bulletin d'Information 228, Lausanne, Switzerland.
- CEN/TC229. (2000): *Precast concrete products - Hollow core slabs for floors - Part 1: Prestressed slabs*.
- FIP. (1998): *Planning and design handbook on precast building structures*, SETO Ltd, Commission on Prefabrication.
- Gabrielsson H. (1999): *Ductility of high performance concrete structures*. Ph. D. Thesis, Division of Structural Engineering, Luleå University of Technology, 1999:15, Luleå, 265 pp.
- Jirásek M. (1999): *Numerical Modeling of Deformation and Failure of Materials*, Short course taught by Milan Jirásek, Rheinisch-Westfälische Technische Hochschule, Aachen.
- Lundgren K. (2002): *Steel-Encased Pull-Through Tests of Seven-Wire Strands*. 02:13, Department of Structural Engineering, Concrete Structures, Chalmers University of Technology, Göteborg, Sweden.
- Pajari M. (1989): *Design of prestressed hollow core slabs*. Research Reports 657, Technical Research Centre of Finland, Espoo.
- Pajari M. (2003a): *Pure torsion test on single slab units*. Internal report RTE50-IR-25/2002, Technical Research Centre of Finland, VTT Building and Transport.
- Pajari M. (2003b): *Shear-torsion interaction tests on single slab units*. Internal report RTE50-IR-1/2003, Technical Research Centre of Finland, VTT Building and Transport.
- TNO. (1998): *DIANA Finite Element Analysis, User's Manual release 7*, TNO Building and Construction Research, Hague.

Appendix A

Below parts of the input files, dat-file, and the execution files, com-fil, used for the analysis of the test ST200E1 in DIANA 7.2 are shown. The input files and the execution files for the analyses of the other tests are similar to these.

Dat-file phase 1 (st200e1-f1-def1.dat)

```
: Model of the test ST200E1 with coarse mesh
: Actual geometries
: 1.03 m of the slab is modelled with solid elements
: the rest of the slab (6.0 m) is modelled with beam elements

KEYWORDS: PRE:FEMGEN
FEMGEN MODEL      : H2C-F1
'COORDINATES'
  1      4.400000E-02      3.999999E-02      0.000000E+00
  2      4.400000E-02      3.999999E-02      -3.000000E-02
  3      4.400000E-02      3.999999E-02      -6.000000E-02
  ...
  ...
  ...
2462     7.7650005E-01     2.140000E-01     -5.300000E-01

'DIRECTIONS'
  1      1.000000E+00     0.000000E+00     0.000000E+00
  2      0.000000E+00     1.000000E+00     0.000000E+00
  3      0.000000E+00     0.000000E+00     1.000000E+00

'ELEMENTS'
CONNECTIVITY
:strands in the solid part
  1 L2TRU  1 2
  2 L2TRU  2 3
  3 L2TRU  4 5
  ...
  ...
  ...
  98 L2TRU 104 105
:beam elements
  99 CL18B 106 107 108
 100 CL18B 108 109 110
 101 CL18B 110 111 112
  ...
  ...
  ...
 113 CL18B 134 135 136
: interface elements between strands and concrete in the solid part
 114 L8IF  137 138 3 2
 115 L8IF  138 139 2 1
 116 L8IF  140 141 6 5
  ...
  ...
  ...
 211 L8IF  241 205 101 70
: Concrete in the solid part
 212 HX24L 142 243 244 245 141 252 254 256
 213 HX24L 248 243 142 246 262 252 141 258
```

```

214 HX24L 242 243 248 247 250 252 262 260
...
...
...
1359 HX24L 2310 2303 2278 2283 2311 2302 2277 2282
: Interface elements between concrete and support plate
1360 Q24IF 319 320 337 336 2312 2313 2316 2315
1361 Q24IF 320 315 327 337 2313 2314 2317 2316
1362 Q24IF 259 260 318 317 2318 2319 2322 2321
...
...
...
1401 Q24IF 611 606 618 628 2373 2374 2377 2376
: Support plate
1402 HX24L 2312 2313 2316 2315 2378 2379 2382 2381
1403 HX24L 2313 2314 2317 2316 2379 2380 2383 2382
1404 HX24L 2318 2319 2322 2321 2384 2385 2388 2387
...
...
...
1443 HX24L 2439 2440 2443 2442 2373 2374 2377 2376
: Loading plates
1444 HX24L 1486 1487 1489 1488 2444 2445 2448 2447
1445 HX24L 1487 1006 1011 1489 2445 2446 2449 2448
1446 HX24L 1488 1489 1491 1490 2447 2448 2451 2450
...
...
...
1451 HX24L 1569 1211 1216 1571 2457 2458 2461 2460
: Loading beam
1500 CL18B 2448 2462 2457

```

MATERI

```

:concrete
/ 99-113 212-1359 /1
:steel
/ 1402-1451 1500 /2
:strands
/ 1-98 /3
:interface (strands)
/ 114-211 /4
:neopren (interface)
/ 1360-1401 /5

```

GEOMETRY

```

:beam
/ 99-113 /1
:strands
/ 1-98 /3
:interface (strands)
/ 114-211 /4
:Loading beam
/1500 /5

```

DATA

```

:beam
/ 99-113 /1

```

'REINFORCEMENT'

LOCATION

```

: Embedded reinforcement in the beam elements, fi 12.9

```

```

40001 BAR
  LOCALY
    / 99-113 / -0.057
  LOCALZ
    / 99-113 / -0.5445
40002 BAR
  LOCALY
    / 99-113 / -0.057
  LOCALZ
    / 99-113 / -0.376
40003 BAR
  LOCALY
    / 99-113 / -0.057
  LOCALZ
    / 99-113 / -0.188
40004 BAR
  LOCALY
    / 99-113 / -0.057
40005 BAR
  LOCALY
    / 99-113 / -0.057
  LOCALZ
    / 99-113 / 0.188
40006 BAR
  LOCALY
    / 99-113 / -0.057
  LOCALZ
    / 99-113 / 0.376
40007 BAR
  LOCALY
    / 99-113 / -0.057
  LOCALZ
    / 99-113 / 0.5445

```

```

MATERI
  / 40001-40020 /3

```

```

GEOMETRY
  / 40001-40020 /3

```

```

'MATERIAL'
:Concrete (from compression test ST200E1b done by VTT)

```

```

1  DENSIT      2.4E+03
   TOTCRK    ROTATE
   POISON      0.15
   YOUNG       3.828E+10
   TENSTR      3.57E+06
   GF1         100.7
   COMSTR      56.4E+06
   TENCRV    HORDYK
   COMCRV    THOREN
   CNFCRV    VECCHI

```

```

:steel
2  DENSIT      7.8E+03
   YOUNG       200.0E9
   POISON      3.0000E-01

```

```

:reinforcement
3  DENSIT      7.8E+03
   YOUNG       198.0E9
   POISON      3.0000E-01

```

```

        YIELD  VMISES
        YLDVAL  1300E6
        HARDEN  STRAIN
:from tensile test done by VTT
        HARDIA  1300E6  0.0
                1600E6  5.9E-3
                1680E6  10E-3
                1730E6  20E-3
                1910E6  50E-3

:Interface Bond-slip for 7-wire
:Pull-through tests by Lundgren (2002)
4  DSTIF  3.90E+13  4.107E+10
    BONDSL  3
    SLPVAL  0  0
            4.07E+6  0.084E-3
            3.04E+6  0.2E-3
            2.65E+6  0.3E-3
            2.39E+6  0.5E-3
            2.36E+6  1.0E-3
            2.51E+6  2.0E-3
            4.0E+6  8.0E-3
            4.0E+6  1.0

:Interface neoprene between concrete and support plate
:from tests done by VTT
5  DSTIF  6.7E+9  6.7E+9

'GEOMETRY'
:beam elements, one hollow core slab unit
:actual geometries
1  ZAXIS  1 0 0
   NZONES 9
   ZONES
:zon 1
        -0.097 -0.5885 -0.097 0.5885
        -0.073 0.5765 -0.073 -0.5765
:zon 2
        0.073 -0.5765 0.073 0.5765
        0.097 0.5765 0.097 -0.5765
:zon 3
        -0.073 -0.5765 -0.073 -0.5475
        0.073 -0.5475 0.073 -0.5765
:zon 4
        -0.073 -0.3925 -0.073 -0.3595
        0.073 -0.3595 0.073 -0.3925
:zon 5
        -0.073 -0.2045 -0.073 -0.1715
        0.073 -0.1715 0.073 -0.2045
:zon 6
        -0.073 -0.0165 -0.073 0.0165
        0.073 -0.0165 0.073 0.0165
:zon 7
        -0.073 0.1715 -0.073 0.2045
        0.073 0.2045 0.073 0.1715
:zon 8
        -0.073 0.3595 -0.073 0.3925
        0.073 0.3925 0.073 0.3595
:zon 9
        -0.073 0.5475 -0.073 0.5765
        0.073 0.5765 0.073 0.5475

```

```

: strands fi 12.5, nominell crosssection 93mm2
3  CROSSE  0.93E-4

: Circumferential area of the reinforcement
4  CONFIG BONDSL
   ZAXIS  1 0 0
   THICK  0.039269908
: Loading beam
5  HINGE PHIZ1 PHIZ2
   RECTAN 0.2 0.1

'DATA'
: Crack band width (taken from observations test SF400C)
1  CRACKB 0.3

'SUPPORTS'
:beam support
 /136 / TR 1 TR 2 RO 3
:loading plate
 /2448 2457 / TR 1 TR 3
:support plate
/2382 2379 2388 2385 2391 2394 2397 2400 2403
 2406 2409 2412 2415 2418 2421 2424 2427 2430
 2433 2436 2439 2442 / TR 1 TR 2

'TYINGS'
ECCENT TR 1 TR 2 TR 3
/ 75 80 85 90 95 100 105 207 212 217 222 227 232
 237 1622 1627 1632 1637 1642 1647 1652 1657
 1662 1667 1672 1677 1682 1687 1692 1697 1702
 1707 1712 1717 1722 1727 1732 1737 1742 1747
 1752 1757 1762 1767 1772 1777 1782 1787 1792
 1797 1802 1807 1812 1817 1826-1827 1832 1837
 1842 1847 1852 1857 1862 1867 1872 1877 1882
 1887 1892 1897 1902 1907 1912 1917 1922 1927
 1932 1937 1942 1947 1952 1957 1962 1967 1972
 1977 1982 1987 1992 1997 2002 2007 2012 2017
 2022 2027 2032 2037 2042 2047 2052 2057 2062
 2067 2072 2077 2082 2087 2092 2097 2102 2107
 2112 2117 2122 2127 2132 2137 2142 2147 2152
 2157 2162 2167 2172 2177 2182 2187 2192 2197
 2202 2207 2212 2217 2222 2227 2232 2237 2242
 2247 2252 2257 2262 2267 2272 2277 2282 2287
 2292 2297 2302 2311 /
:tied to first node in beam
 106

EQUAL TR 1 TR 2
: to prevent the nodes of the strands to move sideways in the
concrete
19  157
16  154
13  151
10  148
7   145
4   142
1   139
3   137
2   138
6   140

```

5	141
9	143
8	144
12	146
11	147
15	149
14	150
18	152
17	153
21	155
20	156
26	158
25	159
24	160
23	161
22	162
31	163
30	164
29	165
28	166
27	167
36	168
35	169
34	170
33	171
32	172
41	173
40	174
39	175
38	176
37	177
46	178
45	179
44	180
43	181
42	182
51	183
50	184
49	185
48	186
47	187
56	188
55	189
54	190
53	191
52	192
58	193
57	194
60	195
59	196
62	197
61	198
64	199
63	200
66	201
65	202
68	203
67	204
70	205
69	206
74	208

73 209
72 210
71 211
79 213
78 214
77 215
76 216
84 218
83 219
82 220
81 221
89 223
88 224
87 225
86 226
94 228
93 229
92 230
91 231
99 233
98 234
97 235
96 236
104 238
103 239
102 240
101 241

'LOADS'

:prestress

CASE 1

ELEMEN

/ 1-98 /

PRESTR 900E6

REINFO

/ 40001-40007 /

PRESTR 900E6

: eccentric point load over two webs, centre nod of loading plate

:for the linear analysis in phase 1

CASE 2

NODAL

/ 2448 2457 / FORCE 2 -0.5E3

:dead weight

CASE 3

WEIGHT

2 -9.8

'END'

Com-file phase 1 (st200e1-f1-def1.com)

```
: First, linear analysis:
*FILOS
  INITIALIZE MA=200000
*INPUT
*PHASE
  BEGIN SELECT
    ELEMEN ALL
  END SELECT
*LINSTA
*NONLIN
  INITIA
  ANALYS PHYSIC
  START PRESTR (1) 1.0 /
  START STRESS.I (1) 1.0 /
  END INITIA
: Defines the loading, load 1 is load 1 in the input file:
LOADIN
  LOAD(1): (1) 1.0 /
  LOAD(2): (2) 1.0 /
  LOAD(3): (3) 1.0 /
  END LOADIN

: Selects what results to save in a Femview result file:
  SELECT
    STEPS 1-20 20-300(2) 300-2000(5) /
  NODES ALL /
  ELEMEN ALL /
  END ELEMEN
  REINFO ALL /
  END REINFO
  END SELECT
  OUTPUT APPEND FEMVIE NONLIN BINARY FI="ST2ED1"
  DISPLA TOTAL GLOBAL
  FORCE RESIDU GLOBAL
  STRAIN TOTAL GREEN GLOBAL
  STRAIN TOTAL GREEN PRINCI
  STRESS TOTAL CAUCHY GLOBAL
  STRESS TOTAL CAUCHY PRINCI
  END OUTPUT

: Carries out the non-linear analysis, defines step sizes and how
many steps:
: Prestressing
  EXECUT START (1) STEPS
  SIZE 0.1(10) /
  PERFOR NEWTON REGULA MI=10
  NORM ENERGY CONTINUE CO=1E-4
  END EXECUT
: Dead weight
  EXECUT LOAD(3) STEPS
  SIZE 1.0(1) /
  PERFOR.R SECANT BFGS MI=10
  NORM ENERGY CONTINUE CO=0.000100
  END EXECUT

*END
```

Dat-file phase 2 (st200e1-f1-def2.dat)

```
PHASE 2
'SUPPORTS'
:Loading point in phase 2 (Middle node of loading beam)
/2462 / TR 2

'LOADS'
:prestress
CASE 1
ELEMEN
/ 1-98 /
      PRESTR 900E6
REINFO
/ 40001-40007 /
      PRESTR 900E6

: Eccentric point loads over two webs,
: middle node of loading beam
: deformation controlled 1mm.
CASE 2
DEFORM
/ 2462 / TR 2 -1.0E-3

: dead weight
CASE 3
WEIGHT
2 -9.8

'END'
```

Com-file phase 2 (st200e1-f1-def2.com)

: Phase 2

```
*INPUT
READ TABLE LOADS
READ APPEND TABLE SUPPOR
```

*PHASE

```
BEGIN SELECT
  ELEMEN ALL
END SELECT
```

INITIA NR=2

*LINSTA

*NONLIN

```
INITIA
ANALYS PHYSIC
END INITIA
```

: Defines the loading, load 1 is load 1 in the input file:

```
LOADIN
LOAD(1): (1) 1.0 /
LOAD(2): (2) 1.0 /
LOAD(3): (3) 1.0 /
END LOADIN
```

: Selects what results to save in a Femview result file:

```
SELECT
  STEPS 1-300 300-2000(5) /
  NODES ALL /
  ELEMEN ALL /
  END ELEMEN
  REINFO ALL /
  END REINFO
END SELECT
OUTPUT APPEND FEMVIE NONLIN BINARY FI="ST2ED2"
DISPLA TOTAL GLOBAL
FORCE RESIDU GLOBAL
STRAIN TOTAL GREEN GLOBAL
STRAIN TOTAL GREEN PRINCI
STRESS TOTAL CAUCHY GLOBAL
STRESS TOTAL CAUCHY PRINCI
END OUTPUT
```

: Carries out the non-linear analysis, defines step sizes and how many steps:

: Dead weight

```
EXECUT START (3) STEPS
SIZE 0.5(10) /
STOP TOTAL 1.
PERFOR NEWTON REGULA MI=10
NORM ENERGY CONTINUE CO=1E-4
END EXECUT
```

: Deformation controlled loading

```
EXECUT LOAD(2) STEPS
SIZE 0.04(200) /
PERFOR SECANT BFGS MI=20
LINE SEARCH
NORM ENERGY CONTIN CO=1E-4
END EXECUT
```

*END